

Two-loop self-energy in the Lamb shift of the ground and excited states of hydrogen-like ions

V. A. Yerokhin

Center for Advanced Studies, Peter the Great St. Petersburg Polytechnic University, 195251 St. Petersburg, Russia

The two-loop self-energy correction to the Lamb shift of hydrogen-like ions is calculated for the $1s$, $2s$, and $2p_{1/2}$ states and nuclear charge numbers $Z = 30-100$. The calculation is performed to all orders in the nuclear binding strength parameter $Z\alpha$. As compared to previous calculations of this correction, numerical accuracy is improved by an order of magnitude and the region of the nuclear charges is extended. An analysis of the Z -dependence of the obtained results demonstrates their consistency with the known $Z\alpha$ -expansion coefficients.

I. INTRODUCTION

Theoretical and experimental investigations of the Lamb shift in atomic systems provide stringent tests of the bound-state quantum electrodynamics (QED) through the first two orders in the fine-structure constant α and to all orders in the nuclear binding strength parameter $Z\alpha$ (where Z is the nuclear charge number) [1, 2]. The main factors presently limiting our theoretical understanding of the Lamb shift in hydrogen-like atoms are [3] the binding two-loop QED effects and, in particular, the two-loop self-energy. Accurate treatment of the two-loop effects is crucial for an adequate comparison of theory and experiment along the whole range of nuclear charge numbers, from hydrogen [4] till lithium-like uranium [5, 6].

The two-loop QED effects were extensively investigated during the last decades, both within the method based on the $Z\alpha$ expansion [7–10] and also within the all-order (in $Z\alpha$) approach [11–15]. Despite significant progress achieved in these studies, at least two important issues remains to be solved. The first is that the extrapolation of the all-order results [15, 16] for the $1s$ two-loop self-energy towards $Z \rightarrow 0$ is only barely consistent with the $Z\alpha$ expansion results [8]. The associated uncertainty is presently the largest theoretical error for the hydrogen Lamb shift [17]. In the foreseeable future (once the proton charge radius puzzle [18] is solved), this error will define the uncertainty of the Rydberg constant, which is determined [17] from the hydrogen spectroscopy. The second issue is that the calculation of Ref. [13] of the two-loop self-energy for the $n = 2$ states was performed only for several ions with $Z \geq 60$. An extension of these calculations towards lower values of Z is needed.

In the present work we report a calculation of the two-loop self-energy correction for the $1s$, $2s$, and $2p_{1/2}$ states of hydrogen-like ions. As compared to previous calculations, we enhance numerical accuracy by an order of magnitude and extend calculations for the $n = 2$ states to lower values of Z , till $Z = 30$. We also present a detailed description of the method of calculation, as developed during two decades of our work on this problem. In our 2003 paper [19] we already reported a detailed analysis of the two-loop self-energy and described the basic scheme of the calculation to all orders in $Z\alpha$. The problem in hand is rather complex and its complete description would be unnecessary long; for this reason, in the present work we will concentrate mainly on new features of the calculational method and only sketch the parts that can be found in Ref. [19].

In the present work we will use the Feynman gauge for the photon propagator since this will make formulas more compact. The actual calculation will be performed for the point distribution of the nuclear charge, although the general analysis will be valid for other nuclear-charge distributions as well. Notations and definitions used throughout the paper are collected in Appendix A. Appendices B and C contain basic notations and formulas for the operator of the electron-electron interaction and the one-loop self-energy, which are essential for this work. We use the relativistic units ($\hbar = c = 1$) and the Heaviside charge units ($\alpha = e^2/4\pi$, $e < 0$).

II. BASIC APPROACH

The two-loop self-energy correction is represented by Feynman diagrams in Fig. 1. The corresponding formal expression can be easily derived, e.g., by the two-time Green function method [2],

$$\Delta E_{\text{SESE}} = \Delta E_{\text{LAL}} + \Delta E_N + \Delta E_O + \Delta E_{\text{red}}. \quad (1)$$

The first term in the right-hand-side of Eq. (1) is the loop-after-loop (LAL) correction induced by the irreducible ($n \neq a$) part of the diagram in Fig. 1(a),

$$\Delta E_{\text{LAL}} = \sum_{n \neq a} \frac{\langle a | \gamma^0 \tilde{\Sigma}(\varepsilon_a) | n \rangle \langle n | \gamma^0 \tilde{\Sigma}(\varepsilon_a) | a \rangle}{\varepsilon_a - \varepsilon_n}, \quad (2)$$

where a denotes the reference state, the summation over n is performed over the spectrum of the Dirac-Coulomb Hamiltonian, ε_a and ε_n are the Dirac-Coulomb energy eigenvalues of the states a and n , respectively, and $\tilde{\Sigma}(\varepsilon) = \Sigma(\varepsilon) - \delta m$ is the one-loop self-energy operator described in Appendix C. The LAL correction can be evaluated by using generalizations of approaches developed for the one-loop self-energy. Such calculations were performed by several groups [20–22]. Since this part of the calculation is relatively straightforward and well established, it will not be described here.

The last three terms in the right-hand-side of Eq. (1) comprise the nontrivial part of the two-loop self-energy, which is the main subject of the present work. The contribution of the

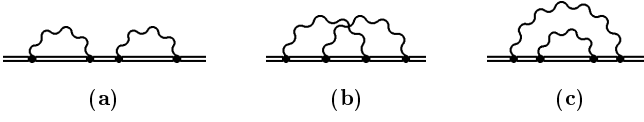


FIG. 1: Two-loop self-energy diagrams. The double line denotes the electron propagating in the binding Coulomb field of the nucleus. The wavy lines denote virtual photons. Individual graphs are referred to as the loop-after-loop (LAL) diagram (a), the overlapping diagram (b), and the nested diagram (c).

overlapping (O) diagram in Fig. 1(b) reads

$$\begin{aligned} \Delta E_O &= (2i\alpha)^2 \int_{C_F} d\omega_1 d\omega_2 \int d\mathbf{x}_1 \dots d\mathbf{x}_4 D(\omega_1, x_{13}) \\ &\times D(\omega_2, x_{24}) \psi_a^\dagger(\mathbf{x}_1) \alpha_\mu G(\varepsilon_a - \omega_1, \mathbf{x}_1, \mathbf{x}_2) \alpha_\nu \\ &\times G(\varepsilon_a - \omega_1 - \omega_2, \mathbf{x}_2, \mathbf{x}_3) \alpha^\mu G(\varepsilon_a - \omega_2, \mathbf{x}_3, \mathbf{x}_4) \\ &\times \alpha^\nu \psi_a(\mathbf{x}_4), \end{aligned} \quad (3)$$

where $x_{ij} = |\mathbf{x}_i - \mathbf{x}_j|$, $\psi_a(\mathbf{x})$ is the reference-state wave function, $D(\omega, \mathbf{x})$ is the scalar part of the photon propagator, $G(\varepsilon, \mathbf{x}_i, \mathbf{x}_j)$ is the Dirac-Coulomb Green function (see Appendix A for notations and definitions), and C_F is the standard Feynman integration contour. The contribution of the nested (N) diagram in Fig. 1(c) is

$$\begin{aligned} \Delta E_N &= (2i\alpha)^2 \int_{C_F} d\omega_1 d\omega_2 \int d\mathbf{x}_1 \dots d\mathbf{x}_4 D(\omega_1, x_{14}) \\ &\times D(\omega_2, x_{23}) \psi_a^\dagger(\mathbf{x}_1) \alpha_\mu G(\varepsilon_a - \omega_1, \mathbf{x}_1, \mathbf{x}_2) \alpha_\nu \\ &\times G(\varepsilon_a - \omega_1 - \omega_2, \mathbf{x}_2, \mathbf{x}_3) \alpha^\nu G(\varepsilon_a - \omega_1, \mathbf{x}_3, \mathbf{x}_4) \\ &\times \alpha^\mu \psi_a(\mathbf{x}_4). \end{aligned} \quad (4)$$

The fourth term in Eq. (1) is the contribution of the reducible ($n = a$) part of the diagram in Fig. 1(a),

$$\Delta E_{\text{red}} = \Delta E_{\text{SE}} \langle a | \gamma^0 \frac{\partial}{\partial \varepsilon} \Sigma(\varepsilon) \Big|_{\varepsilon=\varepsilon_a} | a \rangle, \quad (5)$$

where $\Delta E_{\text{SE}} \equiv \langle a | \gamma^0 \widetilde{\Sigma}(\varepsilon_a) | a \rangle$ is the one-loop self-energy correction described in Appendix C.

Equations (3)-(5) are only formal expressions and need to be renormalized and reformulated, in order to be made suitable for a numerical evaluation. In particular, all ultraviolet (UV) divergences should be regularized in a covariant way and explicitly cancelled. The main problem of the renormalization originates from the fact that the UV divergences are usually identified and cancelled in momentum space, whereas the Dirac-Coulomb Green function is known in the coordinate space and, moreover, in the form of the partial-wave expansion only. There are studies that perform the renormalization of the bound-state QED corrections in coordinate space [23–26], but they are restricted to the one-loop level so far.

In order to covariantly regularize and identify UV divergences present in Eqs. (3)-(5), we use the approach based on the expansion of the Dirac-Coulomb Green function G in

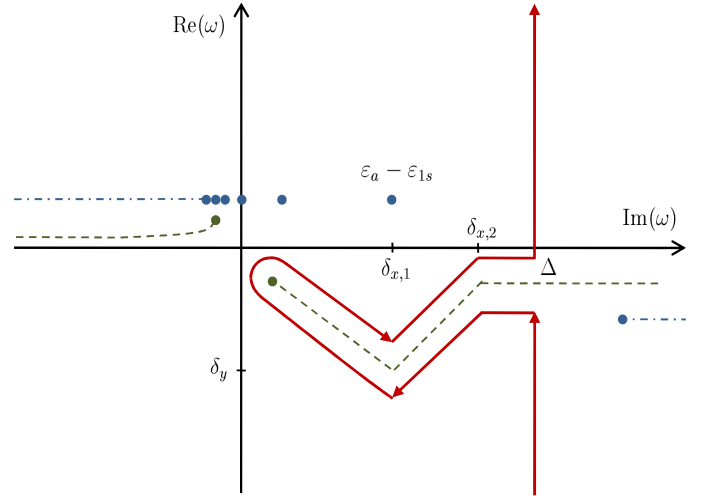


FIG. 2: The integration contour C_{LH} in the complex ω plane. The branch cuts of the photon propagator are shown with the dashed line (green). The poles and the branch cuts of the electron propagator are shown by dots and the dashed-dot line (blue). The poles and branch cuts are shown for the case of the one-loop self-energy of an excited state.

terms of interactions with the binding Coulomb field V ,

$$\begin{aligned} G &= G^{(0)} + G^{(1)} + G^{(2+)} \\ &\equiv G^{(0)} + G^{(0)} V G^{(0)} + G^{(0)} V G^{(0)} V G, \end{aligned} \quad (6)$$

where $G^{(0)}$ is the free Dirac Green function.

In the case of the one-loop self-energy, the renormalization approach is quite straightforward [27]. The UV divergences are induced only by the first two terms of expansion (6). These terms contain only the free Dirac Green function $G^{(0)}$ and are evaluated in momentum space. The remainder does not contain any UV divergences and is evaluated in coordinate space.

For the two-loop self-energy, the renormalization procedure becomes more complicated, mainly because of appearance of mixed terms containing both the UV-divergent subgraphs and the Dirac-Coulomb Green function. The two-loop renormalization procedure based on expansion (6) was first sketched by Mallampalli and Sapirstein [28] and fully realized in our investigations [19, 29]. Following these studies, we split each of the nested, overlapping, and reducible contribution in Eq. (1) into three parts, which are termed as the M , P , and F terms, correspondingly,

$$\Delta E_O = \Delta E_{O,M} + \Delta E_{O,P} + \Delta E_{O,F}, \quad (7)$$

$$\Delta E_N = \Delta E_{N,M} + \Delta E_{N,P} + \Delta E_{N,F}, \quad (8)$$

$$\Delta E_{\text{red}} = \Delta E_{\text{red},M} + \Delta E_{\text{red},P} + \Delta E_{\text{red},F}. \quad (9)$$

The M terms are free from any UV divergences; they are evaluated in coordinate space by using the partial-wave expansions of the Dirac-Coulomb Green functions. The F terms contain only the free Dirac Green functions; they are evaluated in momentum space, without any partial-wave expansions. The P terms contain both the Dirac-Coulomb Green

functions *and* one-loop UV-divergent subgraphs. They are evaluated in the mixed representation: the UV-divergent subgraphs are treated in momentum space, whereas the Dirac-Coulomb Green functions are represented as a Fourier transform over one of the radial variables.

It is convenient to group the M , P , and F terms together, thus representing the two-loop self-energy correction as

$$\Delta E_{\text{SESE}} = \Delta E_{\text{LAL}} + \Delta E_M + \Delta E_P + \Delta E_F, \quad (10)$$

where

$$\Delta E_M = \Delta E_{O,M} + \Delta E_{N,M} + \Delta E_{\text{red},M}, \quad (11)$$

$$\Delta E_P = \Delta E_{O,P} + \Delta E_{N,P} + \Delta E_{\text{red},P}, \quad (12)$$

$$\Delta E_F = \Delta E_{O,F} + \Delta E_{N,F} + \Delta E_{\text{red},F}. \quad (13)$$

The exact definitions of the M , P , and F terms are given in the next three sections.

In our previous investigation [19] we presented a detailed analysis of the divergences arising in individual contributions in Eqs. (11)-(13) and demonstrated their cancellation. In the present work we will rely on that analysis and assume all

UV divergences in individual contributions to be renormalized, i.e., divergent terms $\sim 1/\epsilon$ and $\sim 1/\epsilon^2$ in $D = 4 - 2\epsilon$ dimensions will be dropped out. The reference-state infrared (IR) divergences will be removed from each individual contribution by IR subtractions. The net effect of all IR subtractions is zero, which follows from the analysis of Ref. [19]. So, in our present formulation each of the individual contributions in the right-hand-side of Eqs. (11)-(13) is finite. This fact will greatly simplify the following description.

III. M TERM

The nested, overlapping and reducible M terms are obtained from Eqs. (3)-(5) by applying subtractions that remove all UV and reference-state IR divergences. Each of these terms in turn will be discussed in the next three subsections. In order to keep formulas compact, we will have to repeatedly switch between the Green-function form and the spectral representation of the electron propagators.

A. Nested M term

The nested M term is given by

$$\begin{aligned} \Delta E_{N,M} = & \left(\frac{i}{2\pi}\right)^2 \int_{C_F} d\omega_1 d\omega_2 \left[\sum_{n_1 n_2 n_3} \frac{\langle a n_3 | I(\omega_1) | n_1 a \rangle \langle n_1 n_2 | I(\omega_2) | n_2 n_3 \rangle}{(\epsilon_a - \omega_1 - \epsilon_{n_1})(\epsilon_a - \omega_1 - \omega_2 - \epsilon_{n_2})(\epsilon_a - \omega_1 - \epsilon_{n_3})} \right. \\ & \left. - \frac{1}{\omega_1^2} \sum_{a' a''} \langle a a'' | I(\omega_1) | a' a \rangle \sum_{n_2} \frac{\langle a' n_2 | I(\omega_2) | n_2 a'' \rangle}{\epsilon_a - \omega_2 - \epsilon_{n_2}} - \text{UV subtraction} \right], \end{aligned} \quad (14)$$

where $I(\omega)$ is the operator of the electron-electron interaction defined in Appendix B, the summation over n_i is performed over the complete Dirac spectrum, and intermediate states a' and a'' differ from the reference state a only by the momentum projection. The first term in the brackets in the above formula is the unsubtracted nested contribution given by Eq. (4). The second term in brackets is the IR subtraction that cancels the reference-state IR divergence present in the first term. The third term in the brackets is the UV subtraction that is schematically represented by the following substitution (to be applied both to the first and second terms in the brackets)

$$G_2(\epsilon) \equiv \sum_{n_2} \frac{|n_2\rangle\langle n_2|}{\epsilon - \epsilon_{n_2}} \rightarrow G_2^{(2+)}(\epsilon), \quad (15)$$

where $G^{(2+)}(\epsilon)$ is the Dirac Green function containing two and more interactions with the binding Coulomb field (see Appendix A for the exact definition).

The IR divergence in the unsubtracted nested contribution was discussed in detail in Ref. [19]. It was shown that it appears in the limit $\omega_1 \rightarrow 0$ when both the n_1 and n_3 intermediate states are degenerate in energy with the reference state a , $\epsilon_{n_1} = \epsilon_{n_2} = \epsilon_a$. We now add that the divergences arise only when the n_1 and n_3 intermediate states have the same parity as the reference state a . In particular, for the $a = 2s$ reference state, the contribution of the $n_1 = n_3 = 2p_{1/2}$ intermediate states is IR finite, since the radial integrals in the numerator vanish in the limit $\omega_1 \rightarrow 0$ due to orthogonality of the wave functions. Therefore, the IR divergences originate from the intermediate states $n_1 = a'$ and $n_2 = a''$ that may differ from the reference state a only by the momentum projection ($\mu_{a'}$ and $\mu_{a''}$, respectively). Hence, the the sum over a' and a'' in Eq. (14) is actually the sum over all possible values of $\mu_{a'}$ and $\mu_{a''}$.

In order to bring Eq. (14) to a form suitable for a numerical evaluation, we need to sum over the magnetic substates, perform integrations over the angular variables, and deform the contour of the ω_1 and ω_2 integrations. In the present work we use the same integration contour C_{LH} as for the one-loop self-energy, described in Appendix C and shown in Fig. 2. This contour is similar to the one introduced by P. Mohr in Ref. [30] but differs in details. The fact that we can deform the original contour C_F

to C_{LH} in the two-loop self-energy follows from the analysis presented in Appendix B of Ref. [19]. The resulting expression for the nested M term is

$$\begin{aligned} \Delta E_{N,M} = & \left(\frac{i\alpha}{2\pi} \right)^2 \int_{C_{LH}} d\omega_1 d\omega_2 \left[\sum_{\substack{n_1 n_2 n_3 \\ J_1 J_2}} \frac{(-1)^{J_1+J_2} X_N R_{J_1}(\omega_1, an_3 n_1 a) R_{J_2}(\omega_2, n_1 n_2 n_3)}{(\varepsilon_a - \omega_1 - \varepsilon_{n_1})(\varepsilon_a - \omega_1 - \omega_2 - \varepsilon_{n_2})(\varepsilon_a - \omega_1 - \varepsilon_{n_3})} \right. \\ & \left. - \sum_{J_1} \frac{(-1)^{J_1} R_{J_1}(\omega_1, aaaa)}{\omega_1^2 (2j_a + 1)^2} \sum_{n_2 J_2} \frac{(-1)^{j_2 - j_a + J_2} R_{J_2}(\omega_2, an_2 n_2 a)}{\varepsilon_a - \omega_2 - \varepsilon_{n_2}} - \text{UV subtraction} \right], \end{aligned} \quad (16)$$

where $R_J(\omega, abcd)$ is the relativistic generalization of the Slater radial integral (see Appendix B), X_N is the angular coefficient given by

$$X_N = \frac{(-1)^{j_2 - j_a} \delta_{\kappa_1 \kappa_3}}{(2j_a + 1)(2j_1 + 1)}, \quad (17)$$

j denotes the total angular momentum, and κ is the relativistic angular quantum number of the corresponding electron state.

The expression (16) is finite and can be evaluated numerically as it stands. For the convenience of the numerical computation, however, we divide it in three parts and evaluate each of them separately. First, we single out the contribution with $n_1 = n_2 = n_3 = a$ from the first term in brackets of Eq. (16), together with the corresponding part ($n_2 = a$) of the IR subtraction term. The sum of them is finite but nearly divergent. It can be transformed to a more regular form by performing the integrations over ω_1 and ω_2 , as illustrated in Sec. 1.3 of Ref. [19]. The result is

$$\Delta E_{N,M,a} = \frac{1}{(2j_a + 1)^2} \frac{\alpha^2}{\pi^2} \int_0^\infty dk_1 dk_2 \frac{1}{k_1 k_2 (k_1 + k_2)} \text{Im} \left[\sum_{J_1} (-1)^{J_1} R_{J_1}(k_1, aaaa) \right] \text{Im} \left[\sum_{J_2} (-1)^{J_2} R_{J_2}(k_2, aaaa) \right]. \quad (18)$$

Second, we separate the contribution with $n_1 = n_3 = a$ (but $n_2 \neq a$) from the first term in brackets of Eq. (16), together with the remaining part ($n_2 \neq a$) of the IR subtraction term, and the corresponding part of the UV subtractions. Combining them together, we obtain

$$\begin{aligned} \Delta E_{N,M,i} = & \left(\frac{i\alpha}{2\pi} \right)^2 \int_{C_{LH}} d\omega_1 d\omega_2 \left[\sum_{J_1} \frac{(-1)^{J_1} R_{J_1}(\omega_1, aaaa)}{\omega_1^2 (2j_a + 1)^2} \sum_{\substack{n_2 \neq a \\ J_2}} (-1)^{j_2 - j_a + J_2} R_{J_2}(\omega_2, an_2 n_2 a) \right. \\ & \left. \times \left(\frac{1}{\varepsilon_a - \omega_1 - \omega_2 - \varepsilon_{n_2}} - \frac{1}{\varepsilon_a - \omega_2 - \varepsilon_{n_2}} \right) - \text{UV subtraction} \right]. \end{aligned} \quad (19)$$

This part yields the dominant numerical contribution in the low- Z region but is relatively simple to evaluate and it contains only one partial-wave summation. Finally, the remainder of Eq. (16) is denoted as $\Delta E_{N,M,r}$ and is evaluated separately. This part contains two partial-wave summations and its computation is rather complicated and time consuming. The advantage of evaluating separately $\Delta E_{N,M,r}$ is that it does not suffer (too much) from numerical cancellations occurring in the low- Z region.

B. Overlapping M term

The overlapping M term is can be written as

$$\Delta E_{O,M} = \left(\frac{i}{2\pi} \right)^2 \int_{C_F} d\omega_1 d\omega_2 \left[\sum_{n_1 n_2 n_3} \frac{\langle an_2 | I(\omega_1) | n_1 n_3 \rangle \langle n_1 n_3 | I(\omega_2) | n_2 a \rangle}{(\varepsilon_a - \omega_1 - \varepsilon_{n_1})(\varepsilon_a - \omega_1 - \omega_2 - \varepsilon_{n_2})(\varepsilon_a - \omega_2 - \varepsilon_{n_3})} - \text{UV subtractions} \right], \quad (20)$$

where the first term in the brackets is the unsubtracted overlapping contribution as given by Eq. (3) and the UV subtractions are schematically represented by

$$G_1 G_2 G_3 \rightarrow G_1 G_2 G_3 - G_1 G_2^{(0)} G_3^{(0)} - G_1^{(0)} G_2^{(0)} G_3 + G_1^{(0)} G_2^{(0)} G_3^{(0)} - G_1^{(0)} G_2^{(1)} G_3^{(0)}. \quad (21)$$

Here, the index of G corresponds to the index of n in Eq. (20), i.e., $G_i(\varepsilon) \equiv \sum_{n_i} |n_i\rangle \langle n_i| / (\varepsilon - \varepsilon_{n_i})$.

Summing over the magnetic substates, performing integrations over the angular variables, and deforming the integration contour of the ω_1 and ω_2 integrations, we obtain

$$\Delta E_{O,M} = \left(\frac{i\alpha}{2\pi} \right)^2 \int_{C_{LH}} d\omega_1 d\omega_2 \left[\sum_{\substack{n_1 n_2 n_3 \\ J_1 J_2}} \frac{X_O^{J_1 J_2} R_{J_1}(\omega_1, a n_2 n_1 n_3) R_{J_2}(\omega_2, n_1 n_3 n_2 a)}{(\varepsilon_a - \omega_1 - \varepsilon_{n_1})(\varepsilon_a - \omega_1 - \omega_2 - \varepsilon_{n_2})(\varepsilon_a - \omega_2 - \varepsilon_{n_3})} - \text{UV subtractions} \right], \quad (22)$$

where

$$X_O^{J_1 J_2} = \frac{(-1)^{j_1+j_2+j_3-j_a}}{2j_a+1} \left\{ \begin{matrix} j_2 & J_2 & j_1 \\ j_a & J_1 & j_3 \end{matrix} \right\}. \quad (23)$$

Equation (22) is finite and can be evaluated numerically as it stands. For the convenience of the numerical computation, however, we separate it in several parts and evaluate them separately.

First, we single out the contribution with $n_1 = n_2 = n_3 = a$ and transform it to a more regular form by evaluating the integrations over ω_1 and ω_2 (see Sec. 1.3 of Ref. [19]), with the result

$$\Delta E_{O,M,a} = -\frac{\alpha^2}{\pi^2} \int_0^\infty dk_1 dk_2 \frac{1}{k_1 k_2 (k_1 + k_2)} \times \sum_{J_1 J_2} X_O^{J_1 J_2} \text{Im} \left[R_{J_1}(k_1, aaaa) \right] \text{Im} \left[R_{J_2}(k_2, aaaa) \right]. \quad (24)$$

Second, we separate out the part of $\Delta E_{O,M}$ that is relatively simple, contains only one partial-wave summation, but yields the dominant numerical contribution in the low- Z region, $\Delta E_{O,M,i}$. We define it as a part of the right-hand-side of Eq. (22) with the following restrictions: $\kappa_1 = \kappa_a$, $\kappa_2 = \kappa_3$, $R_{J_1} \rightarrow R_0^C$ (where R_J^C is the Coulomb part of R_J), and the symmetrical contribution with $\kappa_1 = \kappa_2$, $\kappa_3 = \kappa_a$, and $R_{J_2} \rightarrow R_0^C$. The remaining part, $\Delta E_{O,M,r}$, contains two unbound partial wave summations and is evaluated separately. Its computations is the most complicated and time-consuming part of the calculation of the M term.

C. Reducible M term

The reducible M term is given by

$$\Delta E_{\text{red},M} = \Delta E_{\text{SE}} \left(-\frac{i\alpha}{2\pi} \right) \int_{C_F} d\omega \times \left[\sum_n \frac{\langle an | I(\omega) | na \rangle}{(\varepsilon_a - \omega - \varepsilon_n)^2} - \sum_{a'} \frac{\langle aa' | I(\omega) | a'a \rangle}{(-\omega)^2} - \sum_\alpha \frac{\langle a\alpha | I(\omega) | \alpha a \rangle}{(\varepsilon_a - \omega - \varepsilon_\alpha)^2} \right], \quad (25)$$

where ΔE_{SE} is the one-loop self-energy correction to the energy (see Appendix C) and the summation over α is performed over the spectrum of the *free* Dirac Hamiltonian. The first

term in the brackets of the above formula corresponds to the unsubtracted reducible term of Eq. (5), the second term is the IR subtraction, and the third term is the free-electron ($Z = 0$) UV subtraction, $G^{(0)}(\varepsilon) \equiv \sum_\alpha |\alpha\rangle \langle \alpha| / (\varepsilon - \varepsilon_\alpha)$. Expression (25) can be evaluated after deforming the integration contour $C_F \rightarrow C_{LH}$. Its computation is relatively straightforward and was performed by adapting the general scheme developed for the one-loop self-energy matrix element [31].

D. Numerical evaluation of M terms

The general scheme of our numerical computation of the M terms was described in detail in Ref. [19] and does not need to be repeated here. We therefore will concentrate on new features of our computational method. One of the important differences introduced in the present work was the choice of the integration contour for the ω_1 and ω_2 integrations. We now use the contour C_{LH} as described in Appendix C, which has several advantages as compared to the standard Wick rotation ($\omega \rightarrow i\omega$) employed in Ref. [19]. First, by bending the low-energy part of the contour into the complex plane, we avoid the appearance of numerous pole terms, which significantly simplifies the analysis in the case of excited states. Second, this choice of the contour softens the infrared (small- ω) behaviour of the integrand, due to appearance of $\sin(\omega r_{12})$ from the photon propagators, instead of $\exp(-\omega r_{12})$ for the Wick rotation. Because of this, the integrand has a much more regular behaviour at small ω_1 and (or) ω_2 , which significantly simplifies numerical integrations for low values of Z .

Calculations of the $\Delta E_{N,M,i}$ and $\Delta E_{O,M,i}$ parts involve only a single partial-wave expansion over the relativistic angular momentum parameter κ . It was extended up to $|\kappa_{\text{max}}| = 20-22$ and the tail of the expansion was estimated by fitting the expansion terms to the polynomials in $1/|\kappa|$.

Calculations of $\Delta E_{N,M,r}$ and $\Delta E_{O,M,r}$ involve a double partial-wave expansion over κ 's of two (out of the three) electron propagators; we chose them to be κ_1 and κ_3 . An important issue is the extrapolation of $|\kappa_1| \rightarrow \infty$ and $|\kappa_3| \rightarrow \infty$. Following Ref. [19], instead of calculating the matrix of the partial-wave contributions $X_{|\kappa_1|,|\kappa_3|}$ and then extrapolating it, we prefer to work with the matrix $Y_{l_1 l_2}$, where $l_1 = ||\kappa_1| - |\kappa_3|| = 0, 1, \dots$ is the consecutive number of the subdiagonal in the matrix $X_{|\kappa_1|,|\kappa_3|}$ and $l_2 = (|\kappa_1| + |\kappa_3| - l_1)/2 = 1, 2, \dots$ is the consecutive number of the element in the l_1 th subdiagonal of $X_{|\kappa_1|,|\kappa_3|}$. In our computations, we compute the elements of the matrix $Y_{l_1 l_2}$ up to $(l_{1,\text{max}}, l_{2,\text{max}}) = (14, 10)$ for $Z = 30, 40$, and 50 , and $(12, 10)$ for higher values of Z . We

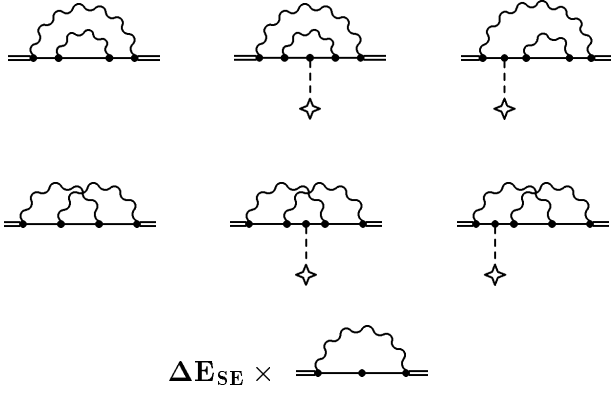


FIG. 3: Feynman diagrams contributing to the F term. The single line denotes the free electron, the double line denotes the bound electron, the dashed line terminated by a cross denotes the interaction with the Coulomb field of the nucleus.

note that for the overlapping diagram $X_{|\kappa_1|,|\kappa_3|} = X_{|\kappa_3|,|\kappa_1|}$, which reduces the number of matrix elements to be computed. The extrapolation was performed in two steps. First, we extrapolate $l_2 \rightarrow \infty$ by fitting the expansion terms to the polynomials in $1/l_2$. Second, we extrapolate $l_1 \rightarrow \infty$ in a similar way.

Numerical results for the M terms for the $1s$, $2s$, and $2p_{1/2}$ states of hydrogen-like ions with $Z = 30-100$ are presented in Table I. The results for the $1s$ state are in agreement with and more accurate than our previous values reported in Ref. [16]. The results for the $2s$ and $2p_{1/2}$ states extend our previous calculations reported in Ref. [13] and improve their accuracy by an order of magnitude.

IV. F TERM

The F term comprises a part of the UV subtraction terms introduced in the M term, namely, those that contain zero or one interaction with the binding Coulomb field in the electron propagators. The corresponding Feynman diagrams are shown in Fig. 3. There are no IR divergences in the F term since the momenta of the initial and the final electron state are off mass-shell and the virtuality $\rho = (m^2 - p^2)/m^2 = (m^2 - \varepsilon_a^2 + \mathbf{p}^2)/m^2$ is strictly positive and never vanishes.

It is natural to separate the F term into the zero-potential F part $\Delta E_{F, \text{zero}}$ (comprising two-loop diagrams with no interactions with the Coulomb field in electron propagators), the one-potential F part $\Delta E_{F, \text{one}}$ (comprising two-loop diagrams with one interaction with the Coulomb field in electron propagators), and the reducible F part $\Delta E_{F, \text{red}}$ (containing derivative of the one-loop diagram),

$$\Delta E_F = \Delta E_{F, \text{zero}} + \Delta E_{F, \text{one}} + \Delta E_{F, \text{red}}. \quad (26)$$

The zero-potential F term can be written as

$$\begin{aligned} \Delta E_{F, \text{zero}} &= \int \frac{d\mathbf{p}}{(2\pi)^3} \psi_a^\dagger(\mathbf{p}) \gamma^0 \Sigma_{\text{zero},R}^{(2)}(p) \psi_a(\mathbf{p}) \\ &\equiv \langle a | \gamma^0 \Sigma_{\text{zero},R}^{(2)} | a \rangle, \end{aligned} \quad (27)$$

where $p = (\varepsilon_a, \mathbf{p})$ is the 4-momentum of the bound electron and $\Sigma_{\text{zero},R}^{(2)}$ is the UV-finite part of the free two-loop self-energy operator $\Sigma_{\text{zero}}^{(2)}(p)$. The separation of UV divergences from the unrenormalized operator $\Sigma_{\text{zero}}^{(2)}(p)$ is performed by working in $D = 4 - 2\epsilon$ dimensions, expanding around $\epsilon = 0$ and identifying divergent $1/\epsilon$ and $1/\epsilon^2$ terms. It was demonstrated [19] that

$$\Sigma_{\text{zero}}^{(2)} - \delta m^{(2)} = (\not{p} - m) B^{(2)} + \frac{\alpha C_\epsilon^2}{4\pi\epsilon} \Sigma_{R,4}^{(0)}(p) + \Sigma_{\text{zero},R}^{(2)}(p), \quad (28)$$

where $\delta m^{(2)}$ is the two-loop mass counterterm, $B^{(2)}$ is the two-loop renormalization constant

$$B^{(2)} = \frac{\alpha^2 C_\epsilon^2}{16\pi^2} \left(-\frac{1}{2\epsilon^2} + \frac{3}{4\epsilon} \right), \quad (29)$$

C_ϵ is the two-loop prefactor

$$C_\epsilon = \Gamma(1 + \epsilon) (4\pi)^\epsilon \left(\frac{\mu^2}{m^2} \right)^\epsilon, \quad (30)$$

and $\Sigma_{R,4}^{(0)}(p)$ is the UV-finite part of the free one-loop self-energy operator in $D = 4$ dimensions. The derivation of the UV-finite part of $\Sigma_{\text{zero},R}^{(2)}(p)$ is discussed in detail in Ref. [19] and will not be repeated here.

The one-potential F term is written as

$$\begin{aligned} \Delta E_{F, \text{one}} &= \int \frac{d\mathbf{p}_1 d\mathbf{p}_2}{(2\pi)^6} \psi_a^\dagger(\mathbf{p}_1) \gamma^0 V(\mathbf{q}) \Sigma_{\text{one},R}^{(2)}(p_1, p_2) \psi_a(\mathbf{p}_2) \\ &\equiv \langle a | V \gamma^0 \Sigma_{\text{one},R}^{(2)} | a \rangle, \end{aligned} \quad (31)$$

where $p_1 = (\varepsilon_a, \mathbf{p}_1)$ and $p_2 = (\varepsilon_a, \mathbf{p}_2)$, $\mathbf{q} = \mathbf{p}_1 - \mathbf{p}_2$, and $\Sigma_{\text{one},R}^{(2)}$ is the UV-finite part of the two-loop vertex operator $\Sigma_{\text{one}}^{(2)}$. It was demonstrated [19] that

$$\Sigma_{\text{one}}^{(2)}(p_1, p_2) = \gamma^0 L^{(2)} + \frac{\alpha C_\epsilon^2}{4\pi\epsilon} \Gamma_{R,4}^0(p_1, p_2) + \Sigma_{\text{one},R}^{(2)}(p_1, p_2), \quad (32)$$

where $\Gamma_{R,4}^\mu(p_1, p_2)$ is the free one-loop vertex operator in $D = 4$ dimensions, and the two-loop renormalization constant $L^{(2)}$ is related to $B^{(2)}$ by the Ward identity, $L^{(2)} = -B^{(2)}$. The derivation of the UV-finite two-loop vertex operator $\Sigma_{\text{one},R}^{(2)}(p)$ is discussed in detail in Ref. [19] and will not be repeated here.

TABLE I: Numerical results for the M contribution ΔE_M , in units of $F(Z\alpha)$ defined in Eq. (61).

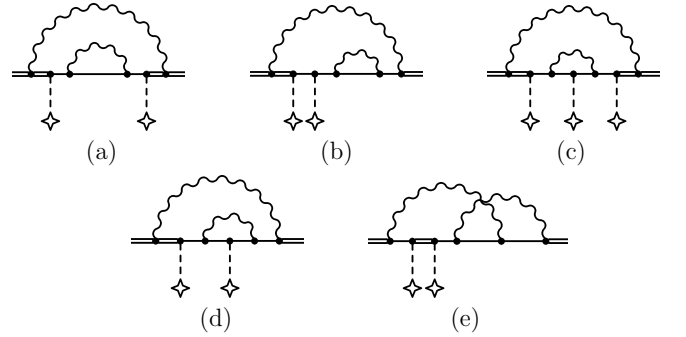
Z	$\Delta E_{\text{red},M}$	$\Delta E_{N,M,i+a}$	$\Delta E_{N,M,r}$	$\Delta E_{O,M,i+a}$	$\Delta E_{M,O,r}$	Total
<i>1s</i>						
30	-1.8191	47.4262	-1.3817 (7)	-58.7732 (6)	-0.922 (2)	-15.470 (2)
40	-1.1463	23.4198	-0.8725 (2)	-29.1977 (2)	-0.458 (2)	-8.255 (2)
50	-0.7824	13.4215 (1)	-0.623 (1)	-16.7579 (1)	-0.261 (1)	-5.003 (2)
60	-0.5649	8.4658	-0.480 (1)	-10.5993 (1)	-0.161 (1)	-3.339 (2)
70	-0.4242	5.7154	-0.394 (2)	-7.2105 (1)	-0.105 (1)	-2.418 (2)
83	-0.3023	3.7005	-0.322 (3)	-4.7746	-0.0654 (8)	-1.764 (3)
92	-0.2395	2.8545	-0.293 (2)	-3.7871	-0.0499 (7)	-1.515 (2)
100	-0.1903	2.3260	-0.2775 (4)	-3.2023	-0.0422 (3)	-1.3864 (5)
<i>2s</i>						
30	-1.9540	87.4704 (5)	-7.305 (5)	-135.761 (6)	-6.27 (1)	-63.82 (1)
40	-1.1141	44.4460 (2)	-4.644 (2)	-70.993 (4)	-3.763 (5)	-36.067 (6)
50	-0.6395	26.3102 (1)	-3.2972 (7)	-42.716 (1)	-2.478 (6)	-22.820 (6)
60	-0.3443	17.2011	-2.5341 (6)	-28.2078 (7)	-1.732 (5)	-15.617 (5)
70	-0.1451	12.0764 (1)	-2.0778 (6)	-19.9526 (4)	-1.272 (1)	-11.371 (1)
83	0.0391	8.2685 (1)	-1.755 (2)	-13.8108 (5)	-0.896 (1)	-8.154 (2)
92	0.1443	6.6512	-1.662 (1)	-11.2475 (5)	-0.727 (1)	-6.842 (2)
100	0.2370	5.6372	-1.670 (1)	-9.7065 (5)	-0.620 (2)	-6.122 (2)
<i>2p_{1/2}</i>						
30	0.0437	107.4798 (4)	-3.696 (7)	-144.371 (5)	-7.137 (7)	-47.68 (1)
40	0.0136	55.1287 (1)	-2.439 (3)	-76.167 (2)	-4.275 (2)	-27.739 (4)
50	-0.0034	32.9318 (1)	-1.7497 (7)	-46.1202 (3)	-2.827 (2)	-17.768 (2)
60	-0.0119	21.7304	-1.3278 (7)	-30.5892 (2)	-1.994 (2)	-12.192 (2)
70	-0.0144	15.4027 (1)	-1.0506 (7)	-21.6861 (1)	-1.466 (3)	-8.814 (3)
83	-0.0111	10.6814	-0.8175 (7)	-14.9849 (2)	-1.015 (3)	-6.147 (3)
92	-0.0053	8.6696	-0.7146 (6)	-12.1248 (2)	-0.793 (2)	-4.968 (2)
100	0.0027	7.4073	-0.6578 (9)	-10.3424 (3)	-0.634 (3)	-4.224 (3)

Finally, the reducible F term can be expressed as [19]

$$\begin{aligned}
\Delta E_{F,\text{red}} = & \Delta E_{\text{SE}} \langle a | \gamma^0 \frac{\partial}{\partial p^0} \Sigma_{R,4}^{(0)}(p) \Big|_{p^0=\varepsilon_a} | a \rangle \\
& - \frac{\alpha}{4\pi} \langle a | \gamma^0 \frac{\partial}{\partial \varepsilon} \frac{\Sigma_{R,D}^{(0)}(p)}{C_\varepsilon} \Big|_{\varepsilon=0} | a \rangle \\
& - \frac{\alpha}{4\pi} \langle a | \gamma^0 V \frac{\partial}{\partial \varepsilon} \frac{\Gamma_{R,D}^0(p_1, p_2)}{C_\varepsilon} \Big|_{\varepsilon=0} | a \rangle, \quad (33)
\end{aligned}$$

where ΔE_{SE} is the one-loop self-energy correction to the energy. The second and the third terms on the right-hand-side of the above equation contain matrix elements of the linear in $\varepsilon \equiv D - 4$ parts of the one-loop operators $\Sigma_{R,D}^{(0)}$ and $\Gamma_{R,D}(p_1, p_2)$ (see Eqs. (248) and (256) of Ref. [19]), which yield finite contributions when multiplied by divergent terms $\sim 1/\varepsilon$ from $\partial/(\partial p^0)\Sigma_D^{(0)}(p)$.

Our numerical approach to the calculation of the F term is described in Ref. [19]. In the present work we use the same method, so it does not need to be discussed here. The computation is relatively straightforward but time-consuming, in particular for the one-potential contribution $\Delta E_{F,\text{one}}$, which involves a 7-fold integration to be performed numerically. As compared to our previous work [19], we adjusted all numerical integrations, employing the extended Gauss-log quadratures [32] alongside with the standard Gauss-Legendre

FIG. 4: Feynman diagrams contributing to the P term.

quadratures, and enhanced the numerical accuracy of the obtained results.

Our numerical results for the F term for the $1s$, $2s$, and $2p_{1/2}$ states of hydrogen-like ions with $Z = 30-100$ are presented in Table II. The numerical accuracy of the listed values is high enough so that it does not influence the total uncertainty of the final results for the two-loop self-energy.

TABLE II: Numerical results for the F term ΔE_F , in units of $F(Z\alpha)$ defined in Eq. (61).

Z	$\Delta E_{F,\text{zero}}$	$\Delta E_{F,\text{one}}$	$\Delta E_{F,\text{red}}$	Total
1s				
30	24.66907 (3)	-16.07999 (8)	36.13890 (1)	44.72798 (9)
40	11.61552 (1)	-9.24107 (3)	17.13164 (1)	19.50609 (3)
50	6.87772 (1)	-6.27573 (2)	9.42434 (1)	10.02633 (2)
60	4.66299 (1)	-4.64818 (2)	5.70902 (1)	5.72383 (2)
70	3.44582 (1)	-3.65961 (1)	3.71093 (1)	3.49714 (1)
83	2.54744 (1)	-2.92278 (1)	2.31342 (1)	1.93808 (2)
92	2.18316 (2)	-2.67665 (1)	1.76914 (4)	1.27566 (5)
100	1.99368 (8)	-2.63549 (3)	1.46677 (3)	0.82496 (9)
2s				
30	90.7129 (2)	-50.90661 (8)	93.50484 (2)	133.3111 (2)
40	39.54636 (4)	-23.2332 (2)	47.42563 (1)	63.7388 (2)
50	21.25492 (1)	-13.56096 (7)	28.03112 (1)	35.72508 (8)
60	13.17901 (3)	-9.28982 (6)	18.32256 (2)	22.21176 (6)
70	9.08349 (1)	-7.12317 (5)	12.89932 (3)	14.85964 (6)
83	6.34101 (1)	-5.76042 (3)	8.94329 (3)	9.52387 (4)
92	5.32624 (3)	-5.41592 (1)	7.33740 (3)	7.24773 (5)
100	4.8297 (2)	-5.49624 (5)	6.41643 (5)	5.7499 (2)
2p_{1/2}				
30	95.6913 (2)	-46.6496 (3)	97.34783 (4)	146.3895 (3)
40	40.76330 (3)	-20.2246 (1)	48.18244 (1)	68.7211 (2)
50	21.48169 (2)	-11.5546 (1)	27.72745 (1)	37.65458 (8)
60	13.16105 (3)	-7.88637 (5)	17.60679 (1)	22.88147 (6)
70	9.05117 (2)	-6.02972 (4)	12.00600 (2)	15.02745 (5)
83	6.38819 (1)	-4.75684 (3)	7.93045 (1)	9.56180 (3)
92	5.43716 (1)	-4.29107 (2)	6.24689 (1)	7.39297 (3)
100	4.98000 (2)	-4.11006 (1)	5.22996 (1)	6.09990 (2)

V. P TERM

The P term comprises the subtractions introduced in the M term that contain two or more interactions with the binding Coulomb field in the electron propagators. (We recall that the subtractions with zero and one interactions with the Coulomb field are already accounted for by the F term.) The Feynman diagrams contributing to the P term are shown in Fig. 4. The distinct feature of these diagrams is that they contain *both* the bound-electron propagators *and* the UV-divergent one-loop subgraphs (the free self-energy loop or the free vertex subgraph). Since in our approach the isolation of UV divergences is performed in momentum space, we have to evaluate the one-loop subgraphs in momentum space. The problem is that to treat the bound-electron propagator (*i.e.*, the Dirac-Coulomb Green function) in momentum space as well does not seem to be practically feasible.

Our solution [29] was to develop a method for computing the Dirac-Coulomb Green function in the mixed coordinate-momentum representation (*i.e.*, one of the radial variables in momentum space and the other radial variable in coordinate space). By now, we developed two different numerical schemes for doing this. In our early works [12, 13, 16, 29] we used the Fourier transformation of the discrete representation

of the spectrum of the Dirac-Coulomb Hamiltonian obtained by the B -spline finite basis set method [33, 34]. This approach is convenient for practical implementations but is plagued by a slow convergence with respect to the size of the basis set, which sets a limitation for the achievable numerical accuracy. In our recent studies [15, 35] we developed a more effective solution of this problem, which involves a numerical Fourier transformation of the analytical representation of the Dirac-Coulomb Green function in terms of the Whittaker functions [1]. This approach provides the Dirac-Coulomb Green function in the mixed coordinate-momentum representation with a high and controllable numerical precision, so that the limiting factor for the accuracy of the final results becomes the convergence of the partial-wave expansion. In Refs. [15, 35] this approach was applied for the ground-state only. In the present work we extend it to the excited states. This extension requires significant modifications of the calculational scheme, which will be described next.

The contribution of Feynman diagrams shown in Fig. 4 is conveniently represented as a sum of three parts

$$\Delta E_P = \Delta E_{N,P,1} + \Delta E_{N,P,2} + \Delta E_{O,P}, \quad (34)$$

which are discussed in turn below.

A. The first nested P contribution

The first nested P contribution is represented by two nested diagrams with the free self-energy loop subgraph, shown in Fig. 4(a) and (b). The corresponding expression can be written as [35]

$$\Delta E_{N,P,1} = \frac{i}{2\pi} \int_{C_F} d\omega \left\{ \sum_{n_1 n_2} \frac{\langle a n_2 | I(\omega) | n_1 a \rangle \langle n_1 V | \mathcal{S}(\varepsilon_a - \omega) | V n_2 \rangle}{(\varepsilon_a - \omega - \varepsilon_{n_1})(\varepsilon_a - \omega - \varepsilon_{n_2})} - \frac{\langle a a'' | I(\omega) | a' a \rangle \langle a' V | \mathcal{S}(\varepsilon_a) | V a'' \rangle}{\omega^2} \right. \\ \left. + 2 \sum_{n_1 \alpha_2 \alpha_3} \frac{\langle a \alpha_2 | I(\omega) | n_1 a \rangle \langle n_1 | V | \alpha_3 \rangle \langle \alpha_3 V | \mathcal{S}(\varepsilon_a - \omega) | \alpha_2 \rangle}{(\varepsilon_a - \omega - \varepsilon_{n_1})(\varepsilon_a - \omega - \varepsilon_{\alpha_3})} \right\}, \quad (35)$$

where the operator \mathcal{S} is defined as

$$\mathcal{S}(\varepsilon) = \frac{1}{\not{p} - m} \Sigma_R^{(0)}(p) \frac{1}{\not{p} - m} \gamma^0 \Big|_{p^0 = \varepsilon}, \quad (36)$$

and $\Sigma_R^{(0)}$ is renormalized free one-loop self-energy operator in $D = 4$ dimensions (see Eq. (C4)). The summations over n_i are performed over the spectrum of the Dirac-Coulomb Hamiltonian, the summations over α_i are performed over the spectrum of the *free* Dirac Hamiltonian, and the states a' and a'' denote the intermediate states that coincide with the reference state a (i.e., $\kappa_{a'} = \kappa_{a''} = \kappa_a$ and $n_{a'} = n_{a''} = n_a$) except for the momentum projections ($\mu_{a'}$ and $\mu_{a''}$, correspondingly). Summations over the magnetic substates (in particular, over $\mu_{a'}$ and $\mu_{a''}$) are implicit. In Eq. (35) we introduced the special notation $|Vn\rangle$ for the product of the nuclear Coulomb potential and the wave function. In coordinate space, it is just

$$|Vn\rangle = V(x) \psi_n(x), \quad \langle nV| = \psi_n^\dagger(x) V(x). \quad (37)$$

In momentum space, $|Vn\rangle$ it is understood as a Fourier transform of the product $V(x) \psi_n(x)$. Matrix elements of \mathcal{S} are assumed to be evaluated in momentum space, whereas matrix operators of the electron-electron interaction operator $I(\omega)$ are assumed to be evaluated in coordinate space.

The first term in the brackets in Eq. (35) corresponds to the diagram in Fig. 4(a), the second term is the IR subtraction that

removes the reference-state IR divergence in the first term, and the third term corresponds to the diagram in Fig. 4(b). We note that the sum over α_2 in the third term $\sum_{\alpha_2} |\alpha_2\rangle \langle \alpha_2|$ is the sum over the complete set of functions; it is inserted artificially for the convenience of representation.

In order to make Eq. (35) suitable for a numerical evaluation, we deform the contour of the ω integration from C_F to a new contour in the complex ω plane. In our previous calculation [35], we used the contour C_{LH} described in Appendix C with $\delta_y = 0$ (since only the ground state was considered in there). In the present work we perform calculations for excited states. In this case there are virtual intermediate states more deeply bound than the reference state. They would cause appearances of the first-order ($\sim 1/(\delta - \omega)$) and second-order ($\sim 1/(\delta - \omega)^2$) singularities on the low-energy part of the C_{LH} contour with $\delta_y = 0$. In our evaluation of the M term, we avoid such singularities by bending the low-energy part of the contour in the complex plane (i.e., using $\delta_y > 0$). For the P term, however, we found the contour with $\delta_y > 0$ to be too difficult for a practical implementation. Instead, we prefer to use the contour C_{LH} with $\delta_y = 0$, treat the double-pole contributions separately, and handle the first-order singularities by evaluating the principal value of the integral. Specifically, we separate out the double-pole contributions $n_1 = n_2 = n$ with $0 < \varepsilon_n < \varepsilon_a$ and calculate them separately, using the standard Wick rotation $\omega \rightarrow i\omega$ of the integration contour.

We thus write Eq. (35) as a sum of two parts, $\Delta E_{N,P,1} = \Delta E_{N,P,1}^a + \Delta E_{N,P,1}^b$, where the second part is the contribution of the $n_1 = n_2 = n$ states with $0 < \varepsilon_n < \varepsilon_a$ and the first part is the remainder. The first term reads

$$\Delta E_{N,P,1}^a = \frac{i}{2\pi} \int_{C_{LH}} d\omega \left\{ \sum_{n_1 n_2} \frac{\langle a n_2 | I(\omega) | n_1 a \rangle \langle n_1 V | \mathcal{S}(\varepsilon_a - \omega) | V n_2 \rangle}{(\varepsilon_a - \omega - \varepsilon_{n_1})(\varepsilon_a - \omega - \varepsilon_{n_2})} - \frac{\langle a a'' | I(\omega) | a' a \rangle \langle a' V | \mathcal{S}(\varepsilon_a) | V a'' \rangle}{\omega^2} \right. \\ \left. + 2 \sum_{n_1 \alpha_2 \alpha_3} \frac{\langle a \alpha_2 | I(\omega) | n_1 a \rangle \langle n_1 | V | \alpha_3 \rangle \langle \alpha_3 V | \mathcal{S}(\varepsilon_a - \omega) | \alpha_2 \rangle}{(\varepsilon_a - \omega - \varepsilon_{n_1})(\varepsilon_a - \omega - \varepsilon_{\alpha_3})} - \sum_n^{0 < \varepsilon_n < \varepsilon_a} \frac{\langle a n'' | I(\omega) | n' a \rangle \langle n' V | \mathcal{S}(\varepsilon_a - \omega) | V n'' \rangle}{(\varepsilon_a - \omega - \varepsilon_n)^2} \right\}. \quad (38)$$

In the above formula, the states $|n'\rangle$ and $|n''\rangle$ have the same energy $\varepsilon_{n'} = \varepsilon_{n''} = \varepsilon_n$ and quantum numbers $\kappa_{n'} = \kappa_{n''} = \kappa_n$ and $n' = n'' = n$, but different values of the momentum projections, $\mu_{n'}$ and $\mu_{n''}$, respectively. Summations over the magnetic substates (including $\mu_{n'}$ and $\mu_{n''}$) are implicit. The subtraction of the last term in the brackets of removes all *second-order* singularities on the low-energy part of the contour. The remaining first-order singularities ($\sim 1/(\delta - \omega)$) were handled by evaluating the principal value of the integral numerically (by using integration quadratures symmetrical with respect to the position of the pole).

The second part $\Delta E_{N,P,1}^b$ is the contribution of the $n_1 = n_2 = n$ states with $0 < \varepsilon_n < \varepsilon_a$. It is transformed by applying the Wick rotation of the contour $\omega \rightarrow i\omega$ and identifying the corresponding pole contributions. The result is

$$\Delta E_{N,P,1}^b = \sum_n^{0 < \varepsilon_n < \varepsilon_a} \left[\langle an'' | I(\Delta_{an}) | n'a \rangle \langle n'V | S'(\varepsilon_n) | Vn'' \rangle - \langle an'' | I'(\Delta_{an}) | n'a \rangle \langle n'V | S(\varepsilon_n) | Vn'' \rangle \right. \\ \left. - \frac{1}{\pi} \text{Re} \int_0^\infty d\omega \frac{\langle an'' | I(i\omega) | n'a \rangle \langle n'V | S(\varepsilon_a - i\omega) | Vn'' \rangle}{(\Delta_{an} - i\omega)^2} \right], \quad (39)$$

where $\Delta_{an} = \varepsilon_a - \varepsilon_n$ and I' and S' denote the derivatives over the energy argument.

In order to evaluate Eqs. (38) and (39) numerically, we rewrite all sums over the Dirac spectrum in terms of the Green functions. In particular, for the first term in the brackets in Eq. (38) we use the representation

$$\sum_{n_1 n_2} \frac{|n_1\rangle \langle n_1 V | S(E) | V n_2 \rangle \langle n_2|}{(E - \varepsilon_{n_1})(E - \varepsilon_{n_2})} = \int \frac{d\mathbf{p}}{(2\pi)^3} G_V(E, \mathbf{x}_1, \mathbf{p}) S(E, \mathbf{p}) G_V(E, \mathbf{p}, \mathbf{x}_2), \quad (40)$$

where G_V denotes the (Fourier transform of the) product GV ,

$$G_V(\varepsilon, \mathbf{x}_1, \mathbf{p}) = \int d\mathbf{x}_2 e^{i\mathbf{p}\cdot\mathbf{x}_2} G(\varepsilon, \mathbf{x}_1, \mathbf{x}_2) V(\mathbf{x}_2), \quad (41)$$

$$G_V(\varepsilon, \mathbf{p}, \mathbf{x}_2) = \int d\mathbf{x}_1 e^{-i\mathbf{p}\cdot\mathbf{x}_1} V(\mathbf{x}_1) G(\varepsilon, \mathbf{x}_1, \mathbf{x}_2). \quad (42)$$

For the third term in the brackets in Eq. (38) we use the following representation

$$\sum_{n_1 \alpha_2 \alpha_3} \frac{|n_1\rangle \langle n_1 V | \alpha_3 \rangle \langle \alpha_3 V | S(E) | \alpha_2 \rangle \langle \alpha_2|}{(E - \varepsilon_{n_1})(E - \varepsilon_{\alpha_3})} = \int \frac{d\mathbf{p}}{(2\pi)^3} G_V^{(1+)}(E, \mathbf{x}_1, \mathbf{p}) \frac{1}{\gamma^0 E - \boldsymbol{\gamma} \cdot \mathbf{p} - m} \Sigma_R^{(0)}(E, \mathbf{p}) G^{(0)}(E, \mathbf{p}, \mathbf{x}_2), \quad (43)$$

where $G_V^{(1+)}$ is the part of G_V with one and more Coulomb interactions, $G_V \equiv G_V^{(0)} + G_V^{(1+)}$.

The main difficulty of the numerical evaluation of the P term is that the computation of the Fourier transform of the Dirac-Coulomb Green function is rather time-consuming (since it is done by evaluating the momentum integration numerically, see Appendix A of Ref. [35] for details). The key idea is to perform the radial integrations over x_1 and x_2 *before* the integration over p . For a given value of p , we compute and store the Fourier transform of the Dirac-Coulomb Green function for all points of the radial x grid that are needed for computation of the radial integrals. The scheme is described in detail in Ref. [35].

A difficulty arises in the numerical evaluation of Eq. (43), due to the presence of the free Green function $G^{(0)}(E, \mathbf{p}, \mathbf{x}_2)$ in the mixed momentum-coordinate representation. For large values of p , $G^{(0)}(E, \mathbf{p}, \mathbf{x}_2)$ is a strongly oscillating function of x_2 . Rapid oscillations cause the radial integration over x_2 to converge slowly and require very dense integration grids. We address this difficulty by noting that $G^{(0)}(E, \mathbf{p}, \mathbf{x}_2)$ can be expressed analytically in terms of the spherical Bessel functions (see Appendix B of Ref. [35]) and thus the integral over x_2 is essentially the Bessel transform of a relatively simple function, which can be computed by the same method as the Fourier transform of the Dirac-Coulomb Green function. By using this approach, we were able to achieve a very good stability of the radial integrations in our computations.

B. The second nested P contribution

The second nested P contribution is represented by nested diagrams containing the free vertex subgraph. They are shown in Fig. 4(c) and (d). The corresponding expression can be written as [35]

$$\Delta E_{N,P,2} = \frac{i}{2\pi} \int_{C_F} d\omega \left\{ \sum_{n_1 n_2} \frac{\langle an_2 | I(\omega) | n_1 a \rangle \langle n_1 V | \mathcal{G}(\varepsilon_a - \omega) | V n_2 \rangle}{(\varepsilon_a - \omega - \varepsilon_{n_1})(\varepsilon_a - \omega - \varepsilon_{n_2})} - \frac{\langle aa'' | I(\omega) | a' a \rangle \langle a' V | \mathcal{G}(\varepsilon_a) | V a'' \rangle}{\omega^2} \right. \\ \left. + 2 \sum_{n_1 \alpha_2} \frac{\langle a\alpha_2 | I(\omega) | n_1 a \rangle \langle n_1 V | \mathcal{G}(\varepsilon_a - \omega) | \alpha_2 \rangle}{\varepsilon_a - \omega - \varepsilon_{n_1}} \right\}, \quad (44)$$

where the operator \mathcal{G} is defined as

$$\mathcal{G}(\varepsilon, \mathbf{p}_1, \mathbf{p}_2) = \frac{1}{\not{p}_1 - m} V(\mathbf{q}) \Gamma_R^0(p_1, p_2) \frac{1}{\not{p}_2 - m} \gamma^0 \Big|_{p_1^0 = p_2^0 = \varepsilon}, \quad (45)$$

$\mathbf{q} = \mathbf{p}_1 - \mathbf{p}_2$, V is the Coulomb potential, and Γ_R^0 is the time component of the renormalized free vertex operator in $D = 4$ dimensions (see Eq. (C5)).

In principle, we could have evaluated Eq. (44) in full analogy with the scheme described for the first nested P term. Such evaluation, however, would be much more time consuming, since matrix elements of the operator \mathcal{G} involve two momentum integrations (over \mathbf{p}_1 and \mathbf{p}_2) and are complicated by the (integrable) Coulomb singularity at $\mathbf{q} = 0$. In order to compute the momentum integrations efficiently, it is desirable to separate out the Coulomb singularity. We achieve this by subtracting and re-adding the vertex operator with the zero transferred momentum and performing one of the momentum integration in the separated contribution analytically. Specifically, we split the vertex operator into the regular (r) and irregular (i) parts with help of Ward identity as

$$\Gamma_R^0(p_1, p_2) = \left[\Gamma_R^0(p_1, p_2) - \frac{1}{2} \Gamma_R^0(p_1, p_1) - \frac{1}{2} \Gamma_R^0(p_2, p_2) \right] + \left[-\frac{1}{2} \Sigma_R^{(0)'}(p_1) - \frac{1}{2} \Sigma_R^{(0)'}(p_2) \right] \equiv \Gamma_r^0(p_1, p_2) + \Gamma_i^0(p_1, p_2), \quad (46)$$

where the prime denotes derivative with respect to p^0 . The regular operator $\Gamma_r^0(p_1, p_2)$ vanishes at $\mathbf{p}_1 = \mathbf{p}_2$, thus removing the Coulomb singularity in the corresponding integral. In the irregular term, the Coulomb singularity is integrated out analytically, by using the Dirac equation and the definition of the Green function. In particular, we make use of the identity

$$\int \frac{d\mathbf{p}_2}{(2\pi)^3} V(\mathbf{q}) \frac{1}{\gamma^0 E - \boldsymbol{\gamma} \cdot \mathbf{p}_2 - m} G_V(E, \mathbf{p}_2, \mathbf{x}_2) = G_V^{(1+)}(E, \mathbf{p}_1, \mathbf{x}_2). \quad (47)$$

The next step is to deform the integration contour of the ω integration, in full analogy with the procedure described for the first nested P contribution, which splits the regular and the irregular terms into the a and b parts. In the result, the second nested P contribution is written as a sum of four terms,

$$\Delta E_{N,P,2} = \Delta E_{N,P,2}^{r,a} + \Delta E_{N,P,2}^{r,b} + \Delta E_{N,P,2}^{i,a} + \Delta E_{N,P,2}^{i,b}, \quad (48)$$

where

$$\begin{aligned} \Delta E_{N,P,2}^{r,a} = & \frac{i}{2\pi} \int_{CLH} d\omega \left\{ \sum_{n_1 n_2} \frac{\langle a n_2 | I(\omega) | n_1 a \rangle \langle n_1 V | \mathcal{G}_r(\varepsilon_a - \omega) | V n_2 \rangle}{(\varepsilon_a - \omega - \varepsilon_{n_1})(\varepsilon_a - \omega - \varepsilon_{n_2})} - \frac{\langle a a'' | I(\omega) | a' a \rangle \langle a' V | \mathcal{G}_r(\varepsilon_a) | V a'' \rangle}{\omega^2} \right. \\ & \left. + 2 \sum_{n_1 \alpha_2} \frac{\langle a \alpha_2 | I(\omega) | n_1 a \rangle \langle n_1 V | \mathcal{G}_r(\varepsilon_a - \omega) | \alpha_2 \rangle}{\varepsilon_a - \omega - \varepsilon_{n_1}} - \sum_n^{0 < \varepsilon_n < \varepsilon_a} \frac{\langle a n'' | I(\omega) | n' a \rangle \langle n' V | \mathcal{G}_r(\varepsilon_a - \omega) | V n'' \rangle}{(\varepsilon_a - \omega - \varepsilon_n)^2} \right\}, \quad (49) \end{aligned}$$

$$\begin{aligned} \Delta E_{N,P,2}^{r,b} = & \sum_n^{0 < \varepsilon_n < \varepsilon_a} \left[\langle a n'' | I(\Delta_{an}) | n' a \rangle \langle n' V | \mathcal{G}'_r(\varepsilon_n) | V n'' \rangle - \langle a n'' | I'(\Delta_{an}) | n' a \rangle \langle n' V | \mathcal{G}_r(\varepsilon_n) | V n'' \rangle \right. \\ & \left. - \frac{1}{\pi} \text{Re} \int_0^\infty d\omega \frac{\langle a n'' | I(i\omega) | n' a \rangle \langle n' V | \mathcal{G}_r(\varepsilon_a - i\omega) | V n'' \rangle}{(\varepsilon_a - i\omega - \varepsilon_n)^2} \right], \quad (50) \end{aligned}$$

$$\begin{aligned} \Delta E_{N,P,2}^{i,a} = & -\frac{i}{2\pi} \int_{CLH} d\omega \left\{ \sum_{n_1 \alpha_1 n_2} \frac{\langle a n_2 | I(\omega) | n_1 a \rangle \langle n_1 V | \alpha_1 \rangle \langle \alpha_1 | \Sigma_R^{(0)'}(\varepsilon_a - \omega) | V n_2 \rangle}{(\varepsilon_a - \omega - \varepsilon_{n_1})(\varepsilon_a - \omega - \varepsilon_{\alpha_1})(\varepsilon_a - \omega - \varepsilon_{n_2})} - \frac{\langle a a'' | I(\omega) | a' a \rangle \langle a' | \Sigma_R^{(0)'}(\varepsilon_a) | V a'' \rangle}{\omega^2} \right. \\ & \left. + \sum_{n_1 \alpha_1 \alpha_2} \frac{\langle a \alpha_2 | I(\omega) | n_1 a \rangle \langle n_1 V | \alpha_1 \rangle \langle \alpha_1 V | \Sigma_R^{(0)'}(\varepsilon_a - \omega) | \alpha_2 \rangle}{(\varepsilon_a - \omega - \varepsilon_{n_1})(\varepsilon_a - \omega - \varepsilon_{\alpha_1})(\varepsilon_a - \omega - \varepsilon_{\alpha_2})} - \sum_n^{0 < \varepsilon_n < \varepsilon_a} \frac{\langle a n'' | I(\omega) | n' a \rangle \langle n' | \Sigma_R^{(0)'}(\varepsilon_a - \omega) | V n'' \rangle}{(\varepsilon_a - \omega - \varepsilon_n)^2} \right\}, \quad (51) \end{aligned}$$

$$\begin{aligned} \Delta E_{N,P,2}^{i,b} = & (-1) \sum_n^{0 < \varepsilon_n < \varepsilon_a} \left[\langle a n'' | I(\Delta_{an}) | n' a \rangle \langle n' | \Sigma_R^{(0)''}(\varepsilon_n) | V n'' \rangle - \langle a n'' | I'(\Delta_{an}) | n' a \rangle \langle n' | \Sigma_R^{(0)'}(\varepsilon_n) | V n'' \rangle \right. \\ & \left. - \frac{1}{\pi} \text{Re} \int_0^\infty d\omega \frac{\langle a n'' | I(i\omega) | n' a \rangle \langle n' | \Sigma_R^{(0)'}(\varepsilon_a - i\omega) | V n'' \rangle}{(\varepsilon_a - i\omega - \varepsilon_n)^2} \right], \quad (52) \end{aligned}$$

where $\mathcal{G}_r(\varepsilon)$ is obtained from Eq. (45) by the substitution $\Gamma_R^0(p_1, p_2) \rightarrow \Gamma_r^0(p_1, p_2)$. Out of the four terms in the right-hand-side of Eq. (48), only the two first ones contain two momentum integrations. They involve the operator \mathcal{G}_r , which is regular at $\mathbf{p}_1 = \mathbf{p}_2$. The last two terms in Eq. (48) contain one momentum integration, and their evaluation is similar to that for the first nested contribution.

For the numerical evaluation, we rewrite Eqs. (49)-(52) in terms of the Green function, identifying, in particular,

$$\sum_{n_1} \frac{|n_1\rangle\langle n_1 V|}{E - \varepsilon_{n_1}} = G_V(E, \mathbf{x}_1, \mathbf{p}_1), \quad (53)$$

$$\sum_{n_1 \alpha_1} \frac{|n_1\rangle\langle n_1 V| \alpha_1 \langle \alpha_1 V|}{(E - \varepsilon_{n_1})(E - \varepsilon_{\alpha_1})} = G_V^{(1+)}(E, \mathbf{x}_1, \mathbf{p}_1). \quad (54)$$

We checked that the expressions with and without the separation (46) give the results consistent with each other within the estimated numerical error.

C. Overlapping P term

The overlapping P term is represented by Feynman diagram in Fig. 4(e). The corresponding expression is written as [35]

$$\begin{aligned} \Delta E_{O,P} = -4i\alpha \int_{C_F} d\omega \int \frac{d\mathbf{p}_1}{(2\pi)^3} \frac{d\mathbf{p}_2}{(2\pi)^3} \int d\mathbf{z} \frac{\exp(-i\mathbf{q} \cdot \mathbf{z})}{\omega^2 - \mathbf{q}^2 + i0} \psi_a^\dagger(\mathbf{z}) \alpha_\mu \\ \times G_V^{(1+)}(\varepsilon_a - \omega, \mathbf{z}, \mathbf{p}_1) \tilde{\Gamma}^\mu(\varepsilon_a - \omega, \mathbf{p}_1; \varepsilon_a, \mathbf{p}_2) \psi_a(\mathbf{p}_2), \end{aligned} \quad (55)$$

where

$$\tilde{\Gamma}^\mu(E, \mathbf{p}_1; \varepsilon_a, \mathbf{p}_2) \equiv \frac{1}{\gamma^0 E - \boldsymbol{\gamma} \cdot \mathbf{p}_1 - m} \Gamma_R^\mu(E, \mathbf{p}_1; \varepsilon_a, \mathbf{p}_2),$$

and Γ_R^μ is the renormalized one-loop free vertex operator in $D = 4$ dimensions (see Eq. (257) of Ref. [19]). In our previous investigations [19, 35] we evaluated Eq. (55) by performing the Wick rotation of the ω integration contour and evaluating separately the pole contributions. For the excited states and low values of the nuclear charges considered in the present work, however, the behaviour of the integrand becomes rather complicated for small ω , acquiring a rapidly changing structure which is difficult to integrate numerically. In order to make the integrand behave more smoothly in the region of small ω , we subtract and re-add the following contribution

$$\begin{aligned} \Delta E_{O,P}^{\text{subtr}} = -4i\alpha \int_{C_F} d\omega \int \frac{d\mathbf{p}_1}{(2\pi)^3} \frac{d\mathbf{p}_2}{(2\pi)^3} \int d\mathbf{z} \frac{\exp(-i\mathbf{q} \cdot \mathbf{z})}{\omega^2 - \mathbf{q}^2 + i0} \psi_a^\dagger(\mathbf{z}) \alpha_\mu \\ \times \sum_k \frac{\psi_k(\mathbf{z}) (\psi_k V)^\dagger(\mathbf{p}_1)}{\varepsilon_a - \omega - \varepsilon_k} \tilde{\Gamma}^\mu(\varepsilon_a, \mathbf{p}_1; \varepsilon_a, \mathbf{p}_2) \psi_a(\mathbf{p}_2), \end{aligned} \quad (56)$$

where the index k run over the virtual bound states with energies $0 < \varepsilon_k < \varepsilon_a + \delta$, where δ is some (reasonably small) positive parameter. It can be immediately seen that we obtained $\Delta E_{O,P}^{\text{subtr}}$ from $\Delta E_{O,P}$ by neglecting ω in the vertex operator and retaining only the lowest-lying virtual bound states in the spectral decomposition of the electron propagator. The summation over k in Eq. (56) thus includes virtual states more deeply bound than the reference state and in addition, virtual states that are close in energy to the reference state. The subtraction of $\Delta E_{O,P}^{\text{subtr}}$ removes the complicated structure of the integrand for small ω . On the other hand, the fact that the vertex operator $\tilde{\Gamma}$ in Eq. (56) does not depend on the energy of the virtual photon ω allows us to perform the integral over ω analytically by the Cauchy theorem.

We thus write

$$\Delta E_{O,P} = (\Delta E_{O,P} - \Delta E_{O,P}^{\text{subtr}}) + \Delta E_{O,P}^{\text{subtr}}.$$

In the first part we make the Wick rotation of the ω integration contour $\omega \rightarrow i\omega$. As a result, this part is separated into the pole term $\Delta E_{O,P}^{\text{pole}}$ and the integral over the imaginary axis, $\Delta E_{O,P}^{\text{Im}}$. In the second part we perform the ω integration analytically by Cauchy theorem. The result is

$$\Delta E_{O,P} = \Delta E_{O,P}^{\text{pole}} + \Delta E_{O,P}^{\text{Im}} + \Delta E_{O,P}^{\text{subtr}}, \quad (57)$$

where

$$\begin{aligned} \Delta E_{O,P}^{\text{pole}} = & -8\pi\alpha \sum_{0 < \varepsilon_n < \varepsilon_a} \int \frac{d\mathbf{p}_1}{(2\pi)^3} \frac{d\mathbf{p}_2}{(2\pi)^3} \int d\mathbf{z} \frac{e^{-i\mathbf{q}\cdot\mathbf{z}}}{(\varepsilon_a - \varepsilon_n)^2 - \mathbf{q}^2 + i0} \psi_a^\dagger(\mathbf{z}) \alpha_\mu \\ & \times \psi_n(\mathbf{z}) (\psi_n V)^\dagger(\mathbf{p}_1) [\tilde{\Gamma}^\mu(\varepsilon_n, \mathbf{p}_1; \varepsilon_a, \mathbf{p}_2) - \tilde{\Gamma}^\mu(\varepsilon_a, \mathbf{p}_1; \varepsilon_a, \mathbf{p}_2)] \psi_a(\mathbf{p}_2), \end{aligned} \quad (58)$$

$$\begin{aligned} \Delta E_{O,P}^{\text{Im}} = & 8\alpha \int_0^\infty d\omega \int \frac{d\mathbf{p}_1}{(2\pi)^3} \frac{d\mathbf{p}_2}{(2\pi)^3} \int d\mathbf{z} \frac{e^{-i\mathbf{q}\cdot\mathbf{z}}}{-\omega^2 - \mathbf{q}^2} \psi_a^\dagger(\mathbf{z}) \alpha_\mu \\ & \times \left[G_V^{(1+)}(\varepsilon_a - i\omega, \mathbf{z}, \mathbf{p}_1) \tilde{\Gamma}^\mu(\varepsilon_a - i\omega, \mathbf{p}_1; \varepsilon_a, \mathbf{p}_2) - \sum_k \frac{\psi_k(\mathbf{z}) (\psi_k V)^\dagger(\mathbf{p}_1)}{\varepsilon_a - i\omega - \varepsilon_k} \tilde{\Gamma}^\mu(\varepsilon_a, \mathbf{p}_1; \varepsilon_a, \mathbf{p}_2) \right] \psi_a(\mathbf{p}_2), \end{aligned} \quad (59)$$

$$\Delta E_{O,P}^{\text{subtr}} = -4\pi\alpha \sum_k \int \frac{d\mathbf{p}_1}{(2\pi)^3} \frac{d\mathbf{p}_2}{(2\pi)^3} \int d\mathbf{z} \frac{e^{-i\mathbf{q}\cdot\mathbf{z}}}{q(\varepsilon_a - q - \varepsilon_k)} \psi_a^\dagger(\mathbf{z}) \alpha_\mu \psi_k(\mathbf{z}) (\psi_k V)^\dagger(\mathbf{p}_1) \tilde{\Gamma}^\mu(\varepsilon_a, \mathbf{p}_1; \varepsilon_a, \mathbf{p}_2) \psi_a(\mathbf{p}_2). \quad (60)$$

The number of states included into the summation over k can be varied; it also serves as a cross-check of the correctness of the numerical procedure. For the ground state we performed calculations with and without the separation of $\Delta E_{O,P}^{\text{subtr}}$; the results were found to be in perfect agreement with each other.

The numerical procedure for evaluation of the P term was described for the $1s$ state in Ref. [35]. This procedure can be directly generalized to the case of excited states considered here. Our numerical results for the P term are presented in Table III. The dominant numerical uncertainty of the listed results comes from the truncation of the partial-wave expansion and extrapolation of the expansion tail.

VI. RESULTS AND DISCUSSION

The two-loop self-energy correction to energy levels is conveniently parameterized in terms of the dimensionless function $F(Z\alpha)$ defined as

$$\Delta E_{\text{SESE}} = m \left(\frac{\alpha}{\pi} \right)^2 \frac{(Z\alpha)^4}{n^3} F(Z\alpha). \quad (61)$$

In the present work we calculate the function $F(Z\alpha)$ to all orders in $Z\alpha$. In order to compare our results with calculations based on the $Z\alpha$ expansion, it is convenient to identify the higher-order remainder function $G_{\text{h.o.}}$ that incorporates contributions of all orders starting with $\alpha^2(Z\alpha)^6$,

$$\begin{aligned} F(Z\alpha) = & B_{40} + (Z\alpha)B_{50} \\ & + (Z\alpha)^2 \left[L^3 B_{63} + L^2 B_{62} + L B_{61} + G_{\text{h.o.}}(Z) \right], \end{aligned} \quad (62)$$

where $L \equiv \ln[(Z\alpha)^{-2}]$ and the expansion of the remainder starts with a constant, $G_{\text{h.o.}}(Z) = B_{60} + Z\alpha(\dots)$. Available results for the expansion coefficients B_{40} - B_{61} [7–10] are summarized in Table I of Ref. [3].

Our numerical results for the two-loop self-energy correction for the $1s$, $2s$, and $2p_{1/2}$ states of H-like ions with $Z = 30$ -100 are presented in Table IV. The last but one column contains our previous results taken from Ref. [16] for the $1s$ state and from Ref. [13] for excited states. As can be seen from the table, the numerical accuracy was improved by an order of magnitude as compared to our previous works and calculations for excited states were extended to the region $Z = 30$ -50. Agreement with our previous calculations is very good. A small deviation in the high- Z region for the $1s$ state is due to the fact that the P -term results in Ref. [16] partly included the finite nuclear size effect, whereas the present results are obtained strictly for the point nucleus.

It is remarkable that, while the total values of the function $F(Z\alpha)$ are quite small numerically (of order of 1 for the s states and of order of 0.1 for the p states), the individual contributions listed in Tables I-III are larger, often by orders of magnitude. So, the final results for the two-loop self-energy are obtained through delicate cancellations of numerous individual contributions to the M , P , and F terms, the cancellations growing fast as Z decreases. Because of the strong Z -dependence of the cancellations, an analysis of the final results for $F(Z\alpha)$ and $G_{\text{h.o.}}(Z)$ as functions of Z and a comparison with the $Z\alpha$ expansion yields an independent check of correctness of the results obtained and of our estimations of errors of the evaluation.

The analysis of the all-order two-loop self-energy results for the $1s$ state and the comparison with the corresponding $Z\alpha$ -expansion coefficients were reported in our previous investigation [15]. In this work we do not repeat this analysis since the improved numerical accuracy for $Z \geq 30$ does not influence the extrapolation to $Z \rightarrow 0$. Instead, we present an analysis for the normalized difference of the two-loop self-energy for the $1s$ and $2s$ states, $\delta E \equiv 8\Delta E_{2s} - \Delta E_{1s}$. This difference is known within the $Z\alpha$ expansion to a much better extent than ΔE_{2s} and ΔE_{1s} separately. Specifically, there are results available for the first two expansion coefficients of the

TABLE III: Numerical results for the P term ΔE_P , in units of $F(Z\alpha)$ defined in Eq. (61).

Z	$\Delta E_{N,P,1}$	$\Delta E_{N,P,2}$	$\Delta E_{O,P}$	Total
1s				
30	-23.8156 (8)	44.810 (2)	-50.408 (2)	-29.413 (2)
40	-9.0139 (4)	17.6060 (8)	-20.1711 (8)	-11.579 (1)
50	-4.3392 (3)	8.4018 (6)	-9.5503 (6)	-5.4877 (9)
60	-2.4456 (2)	4.5451 (4)	-5.0659 (4)	-2.9664 (6)
70	-1.5202 (1)	2.6715 (2)	-2.9353 (3)	-1.7841 (4)
83	-0.8653 (1)	1.4268 (1)	-1.6306 (3)	-1.0690 (4)
92	-0.5542 (1)	0.9091 (1)	-1.1901 (3)	-0.8352 (3)
100	-0.2985 (5)	0.5426 (1)	-0.9791 (3)	-0.7349 (6)
2s				
30	-27.003 (9)	117.320 (8)	-160.260 (8)	-69.94 (1)
40	-3.711 (4)	46.364 (6)	-71.083 (4)	-28.430 (9)
50	1.318 (2)	21.768 (4)	-37.036 (3)	-13.949 (6)
60	2.285 (1)	11.235 (4)	-21.451 (2)	-7.932 (5)
70	2.276 (1)	5.980 (3)	-13.432 (2)	-5.176 (4)
83	2.085 (1)	2.291 (2)	-8.043 (2)	-3.668 (3)
92	2.1074 (8)	0.563 (2)	-6.002 (2)	-3.332 (3)
100	2.3637 (8)	-0.868 (1)	-4.870 (2)	-3.375 (2)
2p_{1/2}				
30	-50.451 (6)	142.357 (7)	-190.46 (1)	-98.56 (1)
40	-11.943 (3)	56.512 (6)	-85.371 (6)	-40.802 (9)
50	-1.854 (2)	26.920 (6)	-44.726 (4)	-19.659 (7)
60	1.063 (1)	14.433 (4)	-25.902 (3)	-10.405 (5)
70	1.827 (1)	8.397 (3)	-16.091 (2)	-5.867 (4)
83	1.8854 (8)	4.482 (2)	-9.359 (2)	-2.992 (3)
92	1.7902 (6)	2.941 (2)	-6.704 (2)	-1.972 (3)
100	1.7531 (7)	1.933 (1)	-5.123 (2)	-1.437 (2)

higher-order remainder,

$$\delta G_{\text{h.o.}}(Z) = \delta B_{60} + (Z\alpha) \ln[(Z\alpha)^{-2}] \delta B_{71} + \dots, \quad (63)$$

where $\delta B_{60} = 14.1$ (4) and $\delta B_{71} = 15.9 \pm 8.0$ [10].

Figure 5 shows our all-order numerical results for the function $\delta F(Z\alpha) = F_{2s}(Z\alpha) - F_{1s}(Z\alpha)$ and the corresponding higher-order remainder $\delta G_{\text{h.o.}}$, in comparison with the $Z\alpha$ -expansion results. We observe that the $Z\alpha$ expansion converges slowly and that the known expansion coefficients are not sufficient in order to describe the all-order results with $Z \geq 30$ even qualitatively. On the other hand, the numerical accuracy and the Z range of the all-order results are not sufficient for extrapolating them to $Z \rightarrow 0$ and making a clear statement about agreement with the $Z\alpha$ expansion. Instead of this, we decided to assume the correctness of the existing $Z\alpha$ -expansion results and to search for the best fitting function that reconciles the $Z\alpha$ -expansion and all-order data. We found that we can describe our numerical data very well by introducing just 3 fitting parameters. As a result, the best fit to our numerical data is found to be

$$\delta G_{\text{h.o.,fit}}(Z) = \delta B_{60} + (Z\alpha) \left\{ \ln[(Z\alpha)^{-2}] \delta B_{71} + b_{70} + (Z\alpha) b_{80} + (Z\alpha)^2 b_{90} \right\}, \quad (64)$$

where the fitted parameters are $b_{70} = -75.324$, $b_{80} = 100.336$, $b_{90} = -49.917$. The fitted function is plotted in Fig. 5 with the dashed-dotted line. Our general conclusion is that our all-order results for the normalized difference of the $2s$ and $1s$ states are consistent with the available $Z\alpha$ -expansion coefficients.

In Fig. 6 we plot our numerical results for the $2p_{1/2}$ state, in comparison with the corresponding $Z\alpha$ -expansion results. We observe that in this case the known terms of the $Z\alpha$ expansion qualitatively reproduce the behaviour of the all-order results for the function $F(Z\alpha)$ in the medium- Z range. The numerical values of the higher-order remainder $G_{\text{h.o.}}$ turn out to be rather small in this case. The accuracy of our all-order results is not sufficient for the extrapolation of $G_{\text{h.o.}}$ to $Z \rightarrow 0$, but we can conclude that there is a qualitative agreement with the $Z\alpha$ expansion for the $2p_{1/2}$ state.

Results for the two-loop self-energy correction for the $2p_{3/2}$ state were reported previously for several high- Z ions [13]. In the present work, we performed calculations for the $2p_{3/2}$ state, the results being consistent with those from Ref. [13]. However, extending our calculations down till $Z = 30$, we found inconsistency with the $Z\alpha$ -expansion results. We assume that this indicates an error in our codes for the $2p_{3/2}$ state, which we were not able to locate so far. For this reason we do not present any results for the $2p_{3/2}$ state in this paper.

TABLE IV: The two-loop self-energy correction, in terms of $F(Z\alpha)$ defined in Eq. (61). $G_{\text{h.o.}}$ is the higher-order remainder function defined by Eq. (62).

Z	ΔE_{LAL}	ΔE_F	ΔE_P	ΔE_M	Total	Previous [13, 16]	$G_{\text{h.o.}}$
1s							
30	-0.7565	44.7280 (1)	-29.413 (2)	-15.470 (2)	-0.912 (3)	-0.90 (3)	-70.39 (7)
40	-0.8711	19.5061	-11.579 (1)	-8.255 (2)	-1.199 (3)	-1.19 (3)	-58.35 (3)
50	-0.9734	10.0263	-5.4877 (9)	-5.003 (2)	-1.438 (2)	-1.44 (3)	-47.42 (2)
60	-1.0825	5.7238	-2.9664 (6)	-3.339 (2)	-1.664 (2)	-1.67 (2)	-37.460 (8)
70	-1.2161	3.4971	-1.7841 (4)	-2.418 (2)	-1.922 (2)	-1.89 (3)	-28.399 (8)
83	-1.4658	1.9381	-1.0690 (4)	-1.764 (3)	-2.361 (3)	-2.35 (1)	-17.798 (9)
92	-1.7342	1.2757	-0.8352 (3)	-1.515 (2)	-2.809 (2)	-2.78 (1)	-11.220 (6)
100	-2.0990	0.8250 (1)	-0.7349 (6)	-1.3864 (5)	-3.3953 (8)	-3.381 (8)	-5.934 (2)
2s							
30	-0.4650 (1)	133.3111 (2)	-69.94 (1)	-63.82 (1)	-0.91 (2)		-57.9 (4)
40	-0.5155	63.7388 (2)	-28.430 (9)	-36.067 (6)	-1.27 (1)		-47.5 (1)
50	-0.5695	35.7251 (1)	-13.949 (6)	-22.820 (6)	-1.613 (8)		-38.19 (6)
60	-0.6434	22.2118 (1)	-7.932 (5)	-15.617 (5)	-1.980 (7)	-1.98 (7)	-29.79 (4)
70	-0.7539	14.8596 (1)	-5.176 (4)	-11.371 (1)	-2.442 (4)	-2.45 (6)	-22.36 (2)
83	-0.9956	9.5239	-3.668 (3)	-8.154 (2)	-3.294 (4)	-3.30 (4)	-13.97 (1)
92	-1.2839	7.2477	-3.332 (3)	-6.842 (2)	-4.209 (3)	-4.22 (3)	-9.086 (7)
100	-1.7071	5.7499 (2)	-3.375 (2)	-6.122 (2)	-5.454 (3)	-5.46 (7)	-5.539 (6)
$2p_{1/2}$							
30	0.0255	146.3895 (3)	-98.56 (1)	-47.68 (1)	0.18 (2)		-0.3 (4)
40	0.0061	68.7211 (2)	-40.802 (9)	-27.739 (4)	0.19 (1)		-0.3 (1)
50	-0.0294	37.6546 (1)	-19.659 (7)	-17.768 (2)	0.198 (7)		-0.24 (5)
60	-0.0814	22.8815 (1)	-10.405 (5)	-12.192 (2)	0.203 (6)	0.22 (7)	-0.18 (3)
70	-0.1524	15.0274	-5.867 (4)	-8.814 (3)	0.193 (5)	0.19 (6)	-0.17 (2)
83	-0.2869	9.5618	-2.992 (3)	-6.147 (3)	0.135 (4)	0.13 (4)	-0.26 (1)
92	-0.4343	7.3930	-1.972 (3)	-4.968 (2)	0.019 (3)	0.01 (3)	-0.444 (8)
100	-0.6512	6.0999	-1.437 (2)	-4.224 (3)	-0.212 (4)	-0.21 (3)	-0.786 (7)

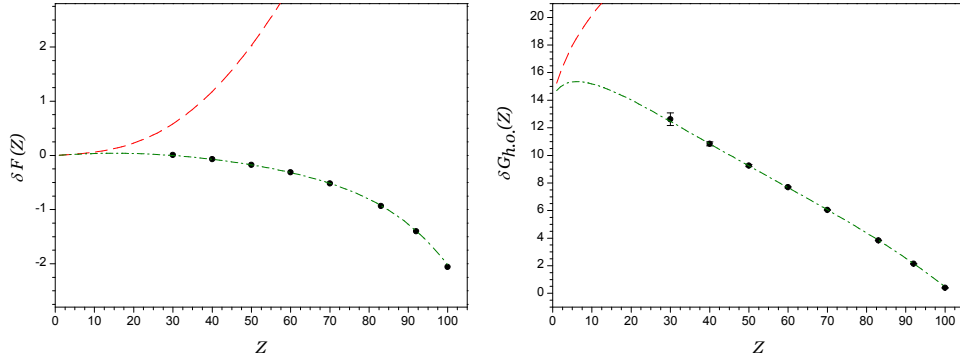


FIG. 5: The two-loop self-energy correction for the normalized difference of the $2s$ and $1s$ states, for the function $\delta F(Z\alpha) = F_{2s}(Z\alpha) - F_{1s}(Z\alpha)$ (left graph) and for the higher-order remainder $\delta G_{\text{h.o.}} = G_{\text{h.o.}}(2s) - G_{\text{h.o.}}(1s)$ (right graph). The dots denote the numerical all-order results, the dashed line (red) represents the $Z\alpha$ -expansion results, the dashed-dotted line (green) shows the best fit of the numerical data.

Conclusion

We carried out calculations of the two-loop self-energy correction to the energy levels of the $1s$, $2s$, and $2p_{1/2}$ states of hydrogen-like ions with the nuclear charges $Z = 30$ -100. The calculation was performed to all orders in the nuclear binding strength parameter $Z\alpha$, for the point distribution of

the nuclear charge. The obtained results improved the accuracy of the previously published values for the two-loop self-energy by an order of magnitude. For excited states, they also extended the lowest nuclear charge range from $Z = 60$ to $Z = 30$. The obtained results were shown to be consistent with the known coefficients of the $Z\alpha$ expansion.

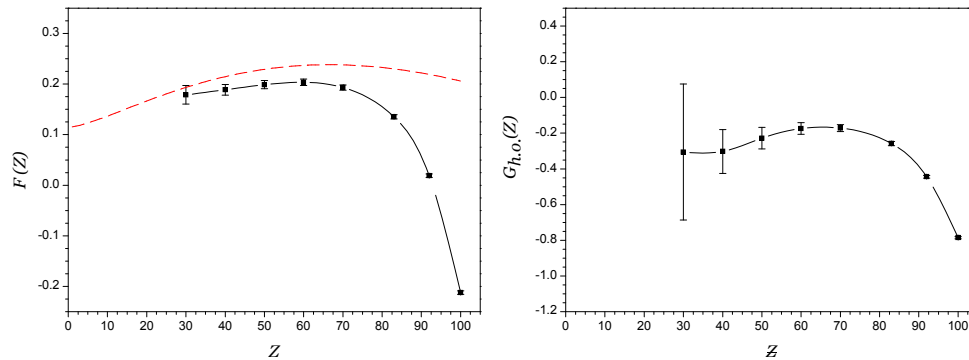


FIG. 6: The two-loop self-energy correction for the $2p_{1/2}$ state, for the function $F(Z\alpha)$ (left graph) and for the higher-order remainder $G_{h.o.}$ (right graph). The dots denote the numerical all-order results, whereas the dashed line (red) represents the $Z\alpha$ -expansion results.

Acknowledgement

No. 3.5397.2017/6.7.

This work was performed with support by the Ministry of Education and Science of the Russian Federation Grant

-
- [1] P. J. Mohr, G. Plunien, and G. Soff, *Phys. Rep.* **293**, 227 (1998).
 [2] V. M. Shabaev, *Phys. Rep.* **356**, 119 (2002).
 [3] V. A. Yerokhin and V. M. Shabaev, *J. Phys. Chem. Ref. Data* **44**, 033103 (2015).
 [4] M. Fischer, N. Kolachevsky, M. Zimmermann, R. Holzwarth, T. Udem, T. W. Hänsch, M. Abgrall, J. Grünert, I. Maksimovic, S. Bize, H. Marion, F. P. D. Santos, P. Lemonde, G. Santarelli, P. Laurent, A. Clairon, C. Salomon, M. Haas, U. D. Jentschura, and C. H. Keitel, *Phys. Rev. Lett.* **92**, 230802 (2004).
 [5] C. Brandau, C. Kozhuharov, A. Müller, W. Shi, S. Schippers, T. Bartsch, S. Böhm, C. Böhme, A. Hoffknecht, H. Knopp, N. Grün, W. Scheid, T. Steih, F. Bosch, B. Franzke, P. H. Mokler, F. Nolden, M. Steck, T. Stöhlker, and Z. Stachura, *Phys. Rev. Lett.* **91**, 073202 (2003).
 [6] P. Beiersdorfer, H. Chen, D. B. Thorn, and E. Träbert, *Phys. Rev. Lett.* **95**, 233003 (2005).
 [7] K. Pachucki, *Phys. Rev. A* **63**, 042503 (2001).
 [8] K. Pachucki and U. D. Jentschura, *Phys. Rev. Lett.* **91**, 113005 (2003).
 [9] A. Czarnecki, U. D. Jentschura, and K. Pachucki, *Phys. Rev. Lett.* **95**, 180404 (2005).
 [10] U. D. Jentschura, A. Czarnecki, and K. Pachucki, *Phys. Rev. A* **72**, 062102 (2005).
 [11] V. A. Yerokhin, *Phys. Rev. Lett.* **86**, 1990 (2001).
 [12] V. A. Yerokhin, P. Indelicato, and V. M. Shabaev, *Phys. Rev. Lett.* **91**, 073001 (2003).
 [13] V. A. Yerokhin, P. Indelicato, and V. M. Shabaev, *Phys. Rev. Lett.* **97**, 253004 (2006).
 [14] V. A. Yerokhin, P. Indelicato, and V. M. Shabaev, *Phys. Rev. A* **77**, 062510 (2008).
 [15] V. A. Yerokhin, *Phys. Rev. A* **80**, 040501(R) (2009).
 [16] V. A. Yerokhin, P. Indelicato, and V. M. Shabaev, *Phys. Rev. A* **71**, 040101(R) (2005).
 [17] P. J. Mohr, D. B. Newell, and B. N. Taylor, *Rev. Mod. Phys.* **88**, 035009 (2016).
 [18] R. Pohl, A. Antognini, F. D. Amaro, F. B. J. M. R. Cardoso, C. A. N. Conde, A. Dax, S. Dhawan, L. M. P. Fernandes, T. W. Hänsch, F. J. Hartmann, V. W. Hughes, O. Huot, P. Indelicato, L. Julien, P. E. Knowles, F. Kottmann, Y.-W. Liu, L. Ludhova, C. M. B. Monteiro, F. Mulhauser, F. Nez, P. Rabinowitz, J. M. F. dos Santos, L. A. Schaller, C. Schwob, D. Taqqu, and J. F. C. A. Veloso, *Can. J. Phys.* **83**, 339 (2005).
 [19] V. A. Yerokhin, P. Indelicato, and V. M. Shabaev, *Eur. Phys. J. D* **25**, 203 (2003).
 [20] A. Mitrushenkov, L. Labzowsky, I. Lindgren, H. Persson, and S. Salomonson, *Phys. Lett. A* **200**, 51 (1995).
 [21] S. Mallampalli and J. Sapirstein, *Phys. Rev. Lett.* **80**, 5297 (1998).
 [22] V. A. Yerokhin, *Phys. Rev. A* **62**, 012508 (2000).
 [23] P. Indelicato and P. J. Mohr, *Phys. Rev. A* **46**, 172 (1992).
 [24] P. Indelicato and P. J. Mohr, *Phys. Rev. A* **58**, 165 (1998).
 [25] P. Indelicato and P. J. Mohr, *Phys. Rev. A* **63**, 052507 (2001).
 [26] P. Indelicato, P. J. Mohr, and J. Sapirstein, *Phys. Rev. A* **89**, 042121 (2014).
 [27] N. J. Snyderman, *Ann. Phys. (New York)* **211**, 43 (1991).
 [28] S. Mallampalli and J. Sapirstein, *Phys. Rev. A* **57**, 1548 (1998).
 [29] V. A. Yerokhin and V. M. Shabaev, *Phys. Rev. A* **64**, 062507 (2001).
 [30] P. J. Mohr, *Ann. Phys. (NY)* **88**, 26 (1974).
 [31] V. A. Yerokhin, K. Pachucki, and V. M. Shabaev, *Phys. Rev. A* **72**, 042502 (2005).
 [32] K. Pachucki, M. Puchalski, and V. Yerokhin, *Comput. Phys. Commun.* **185**, 2913 (2014).
 [33] W. R. Johnson, S. A. Blundell, and J. Sapirstein, *Phys. Rev. A* **37**, 307 (1988).
 [34] V. M. Shabaev, I. I. Tupitsyn, V. A. Yerokhin, G. Plunien, and G. Soff, *Phys. Rev. Lett.* **93**, 130405 (2004).
 [35] V. A. Yerokhin, *Eur. Phys. J. D* **58**, 57 (2010).
 [36] V. A. Yerokhin and V. M. Shabaev, *Phys. Rev. A* **60**, 800 (1999).
 [37] S. A. Blundell, *Phys. Rev. A* **46**, 3762 (1992).

- [38] S. A. Blundell and N. J. Snyderman, Phys. Rev. A **44**, R1427 (1991).
 [39] W. R. Johnson, S. A. Blundell and J. Sapirstein Phys. Rev. A **37**, 2764 (1998).

Appendix A: Definitions, notations and useful identities

The the photon propagator in the Feynman gauge is

$$D_{\mu\nu}(\omega, x_{12}) = g_{\mu\nu} D(\omega, x_{12}) \equiv g_{\mu\nu} \frac{\exp(i\sqrt{\omega^2 + i0}x_{12})}{4\pi x_{12}}, \quad (\text{A1})$$

where $x_{12} = |\mathbf{x}_1 - \mathbf{x}_2|$, and the branch of the square root is fixed by the condition $\text{Im}(\sqrt{\omega^2 + i0}) > 0$.

The Green function of the Dirac-Coulomb equation is defined by its spectral representation

$$G(\varepsilon) = \sum_n \frac{|n\rangle\langle n|}{\varepsilon - \varepsilon_n}, \quad (\text{A2})$$

where the summation over n is performed over the complete spectrum of the Dirac equation with the Coulomb nuclear potential. The free Dirac Green function is the $Z \rightarrow 0$ limit of the Dirac-Coulomb Green function,

$$G^{(0)}(\varepsilon) = \sum_\alpha \frac{|\alpha\rangle\langle\alpha|}{\varepsilon - \varepsilon_\alpha} = G(\varepsilon)|_{Z=0}. \quad (\text{A3})$$

Here and everywhere in this paper, greek subscripts α, β , etc., refer to states of the *free* electron, whereas italic subscripts n, k , etc., to states in the binding Coulomb potential. The one-potential Dirac Green function is defined as the linear in Z term of the Z expansion of the Dirac-Coulomb Green function,

$$G^{(1)}(\varepsilon) = Z \left[\frac{d}{dZ} G(\varepsilon) \right]_{Z=0}. \quad (\text{A4})$$

We introduce special notations for the Dirac Green function containing one and more (two and more) interactions with the binding potential, defined as

$$G^{(1+)}(\varepsilon) = G(\varepsilon) - G^{(0)}(\varepsilon), \quad (\text{A5})$$

$$G^{(2+)}(\varepsilon) = G(\varepsilon) - G^{(0)}(\varepsilon) - G^{(1)}(\varepsilon). \quad (\text{A6})$$

We also mention the identity that follows from the Dirac equation, which is extensively used in this paper. It reads, in coordinate space,

$$\psi_a(\mathbf{x}_1) = \int d\mathbf{x}_2 G^{(0)}(\varepsilon_a, \mathbf{x}_1, \mathbf{x}_2) V(\mathbf{x}_2) \psi_a(\mathbf{x}_2), \quad (\text{A7})$$

where $V(\mathbf{x})$ is the binding Coulomb potential, and in momentum space,

$$\psi_a(\mathbf{p}) = \frac{1}{\gamma^0 \varepsilon_a - \boldsymbol{\gamma} \cdot \mathbf{p} - m} \gamma^0 (V\psi_a)(\mathbf{p}), \quad (\text{A8})$$

where $(V\psi_a)(\mathbf{p})$ is the Fourier transform of the product $V(\mathbf{x})\psi_a(\mathbf{x})$.

Appendix B: Electron-electron interaction operator

The operator of the electron-electron interaction in the Feynman gauge is

$$\begin{aligned} I(\omega) &= e^2 \alpha^\mu \alpha_\mu D(\omega, x_{12}) \\ &= \alpha (1 - \boldsymbol{\alpha}_1 \cdot \boldsymbol{\alpha}_2) \frac{\exp(i\sqrt{\omega^2 + i0}x_{12})}{x_{12}}, \end{aligned} \quad (\text{B1})$$

where $\alpha = e^2/(4\pi)$ is the fine structure constant and $\alpha^\mu = (1, \boldsymbol{\alpha})$ is the vector of Dirac matrices.

The matrix elements of the electron-electron interaction operator is conveniently represented in the form [37, 39]

$$\langle ab|I(\omega)|cd\rangle = \alpha \sum_L J_L(abcd) R_L(\omega, abcd), \quad (\text{B2})$$

where the function J_L contains the standard magnetic-substate dependence of a scalar two-body operator,

$$\begin{aligned} J_L(abcd) &= \sum_{m_L} \frac{(-1)^{L-m_L+j_c-\mu_c+j_d-\mu_d}}{2L+1} \\ &\times C_{j_a\mu_a, j_c-\mu_c}^{Lm_L} C_{j_d\mu_d, j_b-\mu_b}^{Lm_L}, \end{aligned} \quad (\text{B3})$$

$C_{j_1\mu_1, j_2\mu_2}^{jm}$ are the Clebsch-Gordan coefficients and R_L is the relativistic generalization of the Slater radial integral (for explicit expressions see, e.g., Ref. [37] and Appendix C of Ref. [19]). The sum over L in Eq. (B2) is restricted by the triangular selection rules of the Clebsch-Gordan coefficients. It is noteworthy that the operator I preserves the total momentum projection, i.e., the nonzero matrix elements should comply with the requirement

$$\mu_a + \mu_b = \mu_c + \mu_d. \quad (\text{B4})$$

Appendix C: One-loop self-energy

In this section we summarize the main definitions and notations for the one-loop self-energy correction, which are extensively used throughout the paper.

The unrenormalized one-loop self-energy operator is given by

$$\Sigma(\varepsilon, \mathbf{x}_1, \mathbf{x}_2) = 2i\alpha\gamma^0 \int_{C_F} d\omega D(\omega, x_{12}) \alpha_\nu G(\varepsilon - \omega, \mathbf{x}_1, \mathbf{x}_2) \alpha^\nu, \quad (\text{C1})$$

where C_F is the standard Feynman integration contour. The renormalization of the one-loop self-energy is performed [27, 37, 38] by expanding the Dirac-Coulomb Green function G in terms of the interaction with the binding Coulomb field. Using the identity

$$G(\varepsilon) = G^{(0)}(\varepsilon) + G^{(1)}(\varepsilon) + G^{(2+)}(\varepsilon), \quad (\text{C2})$$

one represents the one-loop self-energy correction to the energy as a sum of the zero-potential, one-potential, and many-potential terms, which are induced by the three terms in the

right-hand-side of Eq. (C2), correspondingly,

$$\Delta E_{\text{SE}} = \langle a | \gamma_0 \tilde{\Sigma}(\varepsilon_a) | a \rangle = \Delta E_{\text{SE}}^{\text{zero}} + \Delta E_{\text{SE}}^{\text{one}} + \Delta E_{\text{SE}}^{\text{many}}, \quad (\text{C3})$$

where $\tilde{\Sigma}(\varepsilon) = \Sigma(\varepsilon) - \delta m$ and δm is the corresponding mass counterterm.

The zero-potential term is given by the matrix element of the renormalized free self-energy operator $\Sigma_R^{(0)}(\varepsilon)$ in momentum space,

$$\begin{aligned} \Delta E_{\text{SE}}^{\text{zero}} &= \langle a | \gamma^0 \Sigma_R^{(0)}(\varepsilon_a) | a \rangle \\ &= \int \frac{d\mathbf{p}}{(2\pi)^3} \psi_a^\dagger(\mathbf{p}) \gamma^0 \Sigma_R^{(0)}(\varepsilon_a, \mathbf{p}) \psi_a(\mathbf{p}). \end{aligned} \quad (\text{C4})$$

Explicit formulas for the operator $\Sigma_R^{(0)}(\varepsilon)$ can be found, e.g., in Appendix A of Ref. [36] for the case of $D = 4$ dimensions and in Appendix A.1 of Ref. [19] for the general case of D dimensions.

The one-potential term is given by the matrix element of the renormalized free vertex operator $\Gamma_R^0(\varepsilon_1, \varepsilon_2)$ in momentum space,

$$\begin{aligned} \Delta E_{\text{SE}}^{\text{one}} &= \langle a | V \gamma^0 \Gamma_R^0(\varepsilon_a, \varepsilon_a) | a \rangle \\ &= \int \frac{d\mathbf{p}_1}{(2\pi)^3} \frac{d\mathbf{p}_2}{(2\pi)^3} \psi_a^\dagger(\mathbf{p}_1) V(\mathbf{q}) \gamma^0 \Gamma_R^0(\varepsilon_a, \mathbf{p}_1; \varepsilon_a, \mathbf{p}_2) \psi_a(\mathbf{p}_2), \end{aligned} \quad (\text{C5})$$

where $V(\mathbf{q}) = -4\pi Z\alpha/|\mathbf{q}|$ is the Coulomb potential in the momentum space and $\mathbf{q} = \mathbf{p}_1 - \mathbf{p}_2$. Explicit formulas for the renormalized free vertex operator can be found, e.g., in Appendix B of Ref. [36] for the case of $D = 4$ dimensions and in Appendix A.2 of Ref. [19] for the general case of D dimensions.

The many-potential term is given by the matrix element of the subtracted self-energy operator in coordinate space,

$$\begin{aligned} \Delta E_{\text{SE}}^{\text{many}} &= \langle a | \gamma^0 \left[\Sigma(\varepsilon_a) - \Sigma^{(0)}(\varepsilon_a) - \Sigma^{(1)}(\varepsilon_a) \right] | a \rangle \\ &= 2i\alpha \int_{C_F} d\omega \int d\mathbf{x}_1 d\mathbf{x}_2 D(\omega, \mathbf{x}_{12}) \psi_a^\dagger(\mathbf{x}_1) \\ &\quad \times \alpha_\nu G^{(2+)}(\varepsilon_a - \omega, \mathbf{x}_1, \mathbf{x}_2) \alpha^\nu \psi_a(\mathbf{x}_2). \end{aligned} \quad (\text{C6})$$

In order to bring the many-potential term to the form suitable for a numerical evaluation, one needs to perform the in-

tegrations over the angular variables, sum over the angular-momentum projections, and deform the integration contour. The result [36] can be written down as

$$\begin{aligned} \Delta E_{\text{SE}}^{\text{many}} &= \frac{i\alpha}{2\pi} \int_{C_{LH}} d\omega \left[\sum_{nJ} \frac{(-1)^{J+j_n-j_a}}{2j_a+1} \right. \\ &\quad \left. \times \frac{R_J(\omega, \mathbf{a}nna)}{\varepsilon_a - \omega - \varepsilon_n} - \text{Subtractions} \right], \end{aligned} \quad (\text{C7})$$

where the subtractions are defined symbolically by the substitution

$$G(\varepsilon) \rightarrow G^{(2+)}(\varepsilon), \quad (\text{C8})$$

and the integration contour C_{LH} is shown on Fig. 2. Specifically, the contour C_{LH} consists of the low-energy part C_L and the high-energy part C_H . The high-energy part C_H is parallel to the imaginary axis and extends from $\Delta - i\infty$ to Δ and from Δ to $\Delta + i\infty$. Such a choice of the contour eliminates strong oscillations of the integrand arising in the high-energy region of the contour C_F and replaces them by the exponential falling-off. The low-energy part of the integration contour C_L runs over the upper and the lower banks of the cut of the photon propagator. In the general case of excited reference states, it is also bent in the complex plane in order to avoid singularities coming from virtual bound states with energies $\varepsilon_n < \varepsilon_a$ in the electron propagator. Specifically, the contour C_L consists of the upper and lower parts, both of which extend over 3 sections: $[0, \delta_{x,1} - i\delta_y]$, $[\delta_{x,1} - i\delta_y, \delta_{x,2}]$, and $[\delta_{x,2}, \Delta]$, as shown on Fig. 2. The advantage of such a choice of the low-energy part of the contour is that virtual bound states with the energy $\varepsilon_n \leq \varepsilon_a$ in the electron propagator do not create any pole contributions and do not require any special treatment. The parameters of the contour $\delta_{x,1}$, $\delta_{x,2}$, δ_y , and Δ may be chosen differently. In our recent works, we used the following choice: $\delta_{x,1} = \varepsilon_a - \varepsilon_{1s}$ when the reference state a is an excited state and $\delta_{x,1} = (Z\alpha)^2$ when a is the $1s$ state; $\delta_{x,2} = 2\delta_{x,1}$; $\delta_y = \delta_{x,1}/2$ when there are intermediate states with the energy $\varepsilon_n < \varepsilon_a$ and $\delta_y = 0$ otherwise; and $\Delta = Z\alpha\varepsilon_a$.

We note that for the case when the reference state is the ground state, there is no need to bend the low-energy part of the contour in the complex plane (as there are no intermediate states with energy $0 < \varepsilon_n < \varepsilon_a$), so it is convenient to set $\delta_y = 0$.